https://doi.org/10.5194/acp-2021-487
Preprint. Discussion started: 19 July 2021

Atmospheric Chemistry and Physics Discussions

Oxidation pathways and emission sources of atmospheric particulate nitrate in Seoul: based on $\delta^{15}N$ and $\Delta^{17}O$ of $PM_{2.5}$

Saehee Lim[a], Meehye Lee[a,*], Joel Savarino [b], and Paolo Laj [b]

[a] Dept. of Earth and Environmental Sciences, Korea University, Seoul, 02841, South Korea
[b] Univ. Grenoble-Alpes, CNRS, IRD, Grenoble INP, Institute for Geosciences and Environmental Research (IGE), Grenoble, 38000, France

*Correspondence to: M. Lee (meehye@korea.ac.kr)

Abstract

$PM_{2.5}$ haze pollution driven by secondary inorganic NO_3^- has been a great concern in East Asia. It is, therefore, imperative to identify its sources and oxidation processes, for which nitrogen and oxygen stable isotopes are powerful tracers. Here, we determined the $\delta^{15}N$ (NO_3^-) and $\Delta^{17}O$ (NO_3^-) of $PM_{2.5}$ in Seoul from 2018 to 2019, and estimated quantitatively the relative contribution of oxidation pathways for particulate NO_3^- and major NO_x emission sources. In the range of $PM_{2.5}$ mass concentration from 7.5 μg m^{-3} (summer) to 139.0 μg m^{-3} (winter), the mean $\delta^{15}N$ was -0.7 ± 3.3 ‰ and 3.8 ± 3.7 ‰, and the mean $\Delta^{17}O$ was 23.2 ± 2.2 ‰ and 27.7 ± 2.2 ‰ in the summer and winter, respectively. While OH oxidation was the dominant pathway for NO_3^- during the summer (87 %), nighttime formation via N_2O_5 and NO_3 was more important (38 %) during the winter, when aerosol liquid water content (AWLC) and nitrogen oxidation ratio (NOR) were higher. Interestingly, the highest $\Delta^{17}O$ was coupled with the lowest $\delta^{15}N$ and highest NOR in record-breaking winter $PM_{2.5}$ episodes, revealing the critical role of photochemical oxidation process in severe winter haze development. For NOx sources, vehicle emissions were confirmed as a main contributor, followed by biomass combustion from various activities. The contribution from biogenic soil and coal combustion was slightly increased in summer and winter, respectively. Our results built on multiple-isotope approach provide the first explicit evidence for NO_3^- formation processes and major NOx emission sources in Seoul megacity and suggest an effective mitigation measure to improve $PM_{2.5}$ pollution.

https://doi.org/10.5194/acp-2021-487
Preprint. Discussion started: 19 July 2021

Atmospheric Chemistry and Physics Discussions

Keywords: nitrate, NOx, oxidation processes, emission sources, $PM_{2.5}$ haze, triple oxygen isotope, nitrogen stable isotope

1. Introduction

In Northeast Asia, air pollution characterized by high $PM_{2.5}$ (particulate matters with aerodynamic diameter smaller than 2.5 μm) and ozone concentrations is a cause of public concern due to its serious effects on human health (Lelieveld et al., 2015; Xie et al., 2019). As a result of extensive efforts by East Asian countries to improve the ambient air quality, anthropogenic emissions of SO_x, NO_x, and CO has been significantly reduced, particularly in China (Cheng et al., 2019). Nonetheless, the number of severe haze events and the duration have been increased, which is not understood clearly.

It is also noteworthy that there are common chemical and meteorological characteristics in the occurrence of the $PM_{2.5}$ haze pollution in northeast Asia, such as inorganic species-dominated chemical composition (Lim et al., in reviw; Lim et al., 2020; Liu et al., 2018; Shao et al., 2018; Wang et al., 2019a) and transboundary transport of haze aerosol depending on the synoptic atmospheric circulation (Quan et al., 2020; Shi et al., 2020; Zheng et al., 2019). Overall, approximately 40% of $PM_{2.5}$ consists of NO_3^-, SO_4^{2-}, and NH_4^+ (secondary inorganic aerosol, "SIA") in both urban and background sites in China (Liu et al., 2018) for the period of 2012-2013. The contribution of SIA was further augmented up to 69% at urban Beijing and island sites (Changdao) in North China Plain ("NCP") during the 2016 spring (Lim et al., 2020). A large increase in SIA is particularly associated with efficient formation of NO_3^- in cold months (most frequently in Dec. to Mar.), leading to a rapid increase in $PM_{2.5}$ concentration and developing a persistent haze pollution on a regional scale (Li et al., 2018; Xu et al., 2019). Recent studies suggest that the regional occurrence of the $PM_{2.5}$ haze events derived by NO_3^- across Asian continent has been associated with long-range transport of air pollutants promoted by cold fronts and their intrusion in downward regions by the development of the atmospheric boundary layer (Kang et al., 2019; Lee et al., 2019). However, scientific understanding is still limited because the rapid increase of $PM_{2.5}$ NO_3^- is the result of complex interplay of oxidation and transformation mechanisms producing NO_3^- from various fossil and non-fossil sources of NO_x with micro-to-synoptic meteorology creating the conditions for NO_3^- formation and conversion.

In order to better understand processes of NO_3^- formation including NO_x emission sources in East Asia,

https://doi.org/10.5194/acp-2021-487
Preprint. Discussion started: 19 July 2021

Atmospheric Chemistry and Physics Discussions

a growing number of recent studies have suggested nitrogen and oxygen stable isotope-based measurement as a robust and useful tool for providing important clues for NO_3^- formation as well as NO_x emission sources (He et al., 2018; Lim et al., 2019, 2020; Song et al., 2019; Zong et al., 2017, 2020).

The formation processes of HNO_3 in the atmosphere consist of NO-NO_2 photochemical cycle (R1-R3) and post NO_2 oxidation reactions (R4-R8). During the NO_x cycling, nitrogen isotopic fractionation is affected by unidirectional reactions of Leighton cycle (Leighton cycle isotope effect, LCIE; Li et al., 2020) and NO_x isotope exchange equilibrium (equilibrium isotopic effect, EIE; Li et al., 2020). A recent laboratory experiment has shown that the LCIE associated solely with O_3 reaction (R1) and EIE were -10 ‰ and 28.9 ‰ at room temperature, respectively (Li et al., 2020). The relative importance of these two effects on $\delta^{15}N$ (NO_2) also depends on NO_x levels, leading to increase (decrease) in $\delta^{15}N$ (NO_2) relative to $\delta^{15}N$ (NO_x) values at high (low) NO_x conditions (Kamezaki et al., 2019; Li et al., 2020; Walters et al., 2018). Overall, the nitrogen isotope exchange equilibrium has been suggested to be the dominant fractionation process in NO-NO_2 cycling at urban atmosphere (Freyer et al., 1993) and oxidation reactions forming nitric acid (HNO_3) and particulate NO_3^- (Savarino et al., 2013).

$NO + O_3 \rightarrow NO_2 + O_2$ (R1)

$NO + RO_2 (HO_2) \rightarrow NO_2 + RO (OH)$ (R2)

$NO_2 + h\nu \rightarrow NO + O(^3P)$ (R3)

$NO_2 + OH \rightarrow HNO_3$ (g) (R4)

$NO_2 + O_3 \rightarrow NO_3 + O_2$ (R5)

$NO_2 + NO_3 + M \leftrightarrow N_2O_5$ (R6)

$N_2O_5 + H_2O \xrightarrow{aerosol} 2HNO_3$ (aq) (R7)

$NO_3 + RH \rightarrow HNO_3$ (g) + R (R8)

The kinetic fractionation effect during daytime oxidation of NO_2 to HNO_3 (R4) is relatively minor, being estimated to be -3‰ (Freyer, 1991). During the nighttime when most NO is oxidized to NO_2 without NO_x photolysis, the isotopic equilibrium between NO_2, NO_3, and N_2O_5 (R5-R7) should be achieved. The nighttime thermal equilibrium likely favors the partitioning of ^{15}N into N_2O_5 relative to NO_2 and consequently induces a large isotopic fractionation effect of ~25‰ (R5-R8). On the other hand, the nitrogen partitioning between NO_2 and NO_3 (R5) may induces a negative fractionation effect of

https://doi.org/10.5194/acp-2021-487
Preprint. Discussion started: 19 July 2021

Atmospheric Chemistry and Physics Discussions

~18‰ (Walters and Michalski, 2015). Besides, the major NO_x sources are distinguished in their nitrogen isotopic compositions; biogenic soil (driven by fertilizer use; -35.1‰ ± 10.2‰) (Felix and Elliott, 2014; Li and Wang, 2008; Yu and Elliott, 2017), biomass burning (1.8‰ ±1.8‰) (Fibiger and Hastings, 2016), vehicle emissions (-2.5‰ ± 1.5‰) (Walters et al., 2015), and coal combustion (14.2‰ ± 4.5‰) (Felix et al., 2012; Heaton, 1990). Exploiting these properties, $\delta^{15}N$ can be used for NO_x source apportionment based on the fact that measured $\delta^{15}N$ (NO_3^-) is affected by isotope fractionation effects during photochemical cycling of NO-NO_2 and NO_2 post oxidation and by $\delta^{15}N$ of NO_x emission sources. Therefore, the isotope fractionation effects should be first evaluated to accurately quantify the contribution of NO_x emission sources.

Lately, $\Delta^{17}O$ (NO_3^-) has been used for tracing NO_3^- oxidation pathways (Alexander et al., 2009, 2020; Morin et al., 2009; Savarino et al., 2007, 2013). In O_3 formation reactions, a rare isotope effect leads to excess ^{17}O enrichment relative to what is expected based on the ^{18}O enrichments (Thiemens, 2006). This mass-independent $\Delta^{17}O$ signature of O_3 (^{17}O-excess, defined as $\delta^{17}O - 0.52 \times \delta^{18}O$) is transferred to NO_x during oxidation processes, which enables the $\Delta^{17}O$ (NO_3^-) to serve as a conservative marker to track the chemical formation of NO_3^-. Photochemical formation by HO_x radicals (OH, HO_2, RO_2) leads to a relatively low $\Delta^{17}O$ (NO_3^-), whereas nighttime formation through N_2O_5 and NO_3 results in high $\Delta^{17}O$ (Alexander et al., 2009, 2020; Michalski et al., 2003; Morin et al., 2009). Consequently, the difference in $\Delta^{17}O$ (NO_3^-) suggests approaching a proportional contribution of daytime and nighttime oxidation of NO_3^-.

Recently, several studies have used $\Delta^{17}O$ (NO_3^-) measurements for quantifying NO_3^- oxidation pathways (He et al., 2018; Wang et al., 2019b) or $\delta^{15}N$ (NO_3^-) measurements for apportioning NO_x emission sources (Chang et al., 2018; Kawashima, 2019; Li et al., 2019; Lim et al., 2020; Song et al., 2019; Zong et al., 2020) in China. However, to date, few field studies have coupled $\delta^{15}N$ (NO_3^-) and $\Delta^{17}O$ (NO_3^-) to investigate emission sources of NO_x and NO_x-to-NO_3^- oxidation processes, e.g., a study in Japan (Nelson et al., 2018) and a study in west Virginia USA (Rose et al., 2019).

In this study, we present the measurement results of $\delta^{15}N$ and $\Delta^{17}O$ of NO_3^- in Seoul from 2018 to 2019, during which we encountered the record-breaking $PM_{2.5}$ concentrations. Then, the $\delta^{15}N$ and $\Delta^{17}O$ measurements are used to evaluate seasonally distinct atmospheric oxidation pathways of NO_3^- and to quantify the relative contribution of major NO_x emission sources in the study region.

https://doi.org/10.5194/acp-2021-487
Preprint. Discussion started: 19 July 2021


Atmospheric Chemistry and Physics Discussions

2. Measurements and methods

2.1. Sampling

We collected $PM_{2.5}$ filter samples on the rooftop of six-story Asan science building at Korea University campus located in northeast Seoul, the capital of South Korea (37.59° N, 127.02° E; Figure S1) during the summer 2018 (26 May to 22 Aug.; n = 13) and the winter 2018-2019 (27 Dec. to 3 Mar.; n = 18). Seoul is a metropolitan area with a population of 9.77 million and known to be influenced by heavy road traffic all around. The $PM_{2.5}$ particulates were collected on quartz filters (20 cm x 25 cm ; Pallflex Products, Putnam, USA) at a nominal flow rate of 96 m^3 hr^{-1} for 1 to 3 days using a high-volume air sampler (3000 series, Ecotech, Australia). Filters were analyzed for water-soluble ions, carbonaceous compounds, total nitrogen (TN) and carbon (TC), and stable nitrogen and oxygen isotopic ratios. Reactive gases including O_3, NO, NO_2, SO_2, and CO, and meteorological suite including air temperature, relative humidity, and wind speed and direction were measured hourly at the campus and nearby monitoring sites run by the National Institute of Environmental Research (NIER) and the Korea Meteorological Administration (KAM), respectively. Additionally, the hourly concentration of NH_3 was adopted from a previous study (NIER, 2019), which covers May to Aug. 2018. These dates were averaged daily for comparison with filter-based chemical composition data, if necessary.

2.2. Chemical analyses

Filters were stored in a freezer pending chemical analysis. Chemical composition of $PM_{2.5}$ was determined for 8 water-soluble ions (Cl^-, NO_3^-, SO_4^{2-}, Na^+, NH_4^+, K^+, Ca^{2+}, and Mg^{2+}) by ion chromatography (IC; Eco-IC, Metrohm, Switzerland); OC and EC by an OC analyzer (Sunset Laboratory Inc., US) using the thermo-optical transmittance method (NIOSH870); water-soluble organic carbon (WSOC) by a total organic carbon (TOC) analyzer (TOC-L, Shimadzu; at the Korea Basic Science Institute); and TC and nitrogen (TN) by an elemental analyzer (EA, Fisons NA-1500NC, Thermo, Waltham, MA, USA). Mass concentrations of these constituents were corrected for laboratory and field blanks. The detection limit, determined as three standard deviations (SD) above blank concentrations, was <0.1 ppm for ionic species, 0.5 μg cm^{-3} for TC, and 4 ppb for TOC. Details of the analytical methods can be found elsewhere (Lim et al., 2020).

Following the bacterial denitrifier method (Casciotti et al., 2002), the $\Delta^{17}O$ of NO_3^- was measured simultaneously with $\delta^{18}O$ and $\delta^{15}N$ coupled with an IRMS measurement using an in-house peripheral system at the Université Grenoble Alpes (Morin et al., 2009). In brief, NO_3^- of samples was converted

https://doi.org/10.5194/acp-2021-487
Preprint. Discussion started: 19 July 2021


Atmospheric Chemistry and Physics Discussions

to N_2O via bacterial denitrification and the N_2O was further converted into O_2 and N_2, which were separated via a gas chromatography column before being introduced to the IRMS system. Samples were measured in batch with reference materials following strictly the identical treatment principles, including the same water matrix for standards and samples. Together with samples, a subset of international nitrate reference materials (US Geological Survey 32, 34, and 35, as well as their mixtures) was measured for correction and calibration of $\Delta^{17}O$ and $\delta^{18}O$ values relative to VSMOW and $\delta^{15}N$ values relative to air N_2. The uncertainties (1σ) for $\Delta^{17}O(NO_3^-)$ $\delta^{15}N(NO_3^-)$ were 0.4‰ and 0.3‰, respectively. Details of the method can be found in Morin et al. (2009).

2.3. Quantifying isotope fractionation effects

2.3.1. Isotope fractionation effects of NO_2 oxidation to atmospheric particulate NO_3^- : $\delta^{15}N$ (NO_3^-)

Throughout two main steps of HNO_3 formation in the atmosphere (NO_x photochemical cycling (R1-R3) and post NO_2 oxidation reactions (R4-R8)), three major pathways of HNO_3 formation include (i) OH pathway, (ii) O_3 pathway associated with N_2O_5, and (iii) O_3 pathway associated with NO_3.

OH pathway

During the daytime, the photochemical equilibrium between NO and NO_2 is achieved within several minutes. When NO and NO_2 coexist in similar quantities due to the Leighton cycle, ^{15}N is preferentially partitioned into NO_2 via the equilibrium isotope effect, leading to higher $\delta^{15}N$ in NO_2 relative to NO and NO_x (Freyer et al., 1993; Walters et al., 2016). Considering the comparable concentrations of NO and NO_2 over a year in Seoul (Figure S3), the isotope effects on $\delta^{15}N$ (NO_3^-) should be significantly affected by NO_x photochemical interactions. The relative importance of EIE and LCIE to $\delta^{15}N(NO_2)$ can be assessed by comparing lifetimes of NO_2 with respect to isotope exchange with NO ($\tau_{exchange}$) and photolysis (τ_{NO2+hv}). In this regard, the "A" factor was defined as $\tau_{exchange}/\tau_{NO2+hv} = j_{NO2}/ k_1 \times [NO]$ (k_1= 8.14×10^{-14} cm^3 s^{-1}, Sharma et al., 1970) by Li et al. (2020, 2021). These studies demonstrated that A was as small as 0.01-0.5 in EIE-dominated regime with $NO_x > 20$ ppbv and the ratio of NO_2/NO_x <0.6. In Seoul, A factor was estimated to be 0.08 ± 0.20 (median ± standard deviation) and 0.60 ± 0.51 during the winter and summer months, respectively, indicating the significant influence of the equilibrium isotope effect on NO-NO_2 isotopic fractionation. The time series j_{NO2} was calculated using the Master

https://doi.org/10.5194/acp-2021-487
Preprint. Discussion started: 19 July 2021


Atmospheric Chemistry and Physics Discussions

Chemical Mechanisms (MCM) (Saunders et al., 2003) model.

After photochemical NO_x photochemical cycling, NO_2 is oxidized by the reaction with OH radical to form atmospheric HNO_3 ("HNO_3 (1) pathway"). Assuming no kinetic isotope effects associated with HNO_3 (1) pathway that should be minor (-3‰), the N fractionation effect of particulate NO_3^- produced via HNO_3 (1) pathway (ε_1, unit in ‰) can be expressed as the following (Walters and Michalski, 2016):

$$\delta^{15}N\ (HNO_3)\ (1) = \delta^{15}N\ (NO_2) = \delta^{15}N\ (NO_x) + \varepsilon_1 \quad \text{(Eq. 1-1)}$$

$$\varepsilon_1 = 1000\ ((^{15}\alpha_{NO2/NO} - 1)\ (1 - f_{NO2}))/\ ((1 - f_{NO2}) + (^{15}\alpha_{NO2/NO} \times f_{NO2})) \quad \text{(Eq. 1-2)}$$

, where f_{NO2} is the fraction of NO_2 relative to the total NO_x, and $^{15}\alpha_{NO2/NO}$ is the isotope fractionation factor for NO_2/NO associated with NO_x photochemical cycling. We adopted the $^{15}\alpha_{NO2/NO}$ of 1.018, a combined NO-NO_2 isotope fractionation factor, that was derived from the field measurement of NO_x and $\delta^{15}N\ (NO_2)$ at Julich over a year (Freyer et al., 1993). Later, it was confirmed through a chamber simulation experiment (Li et al., 2020). In the present study, the measured f_{NO2} was used individually for summer samples and a seasonal mean f_{NO2} (0.69) was applied to winter samples due to the availability of NO-NO_2 measurement data.

Oxidation of NO_x to HNO_3 is regarded as the formation pathway of particulate NO_3^- via the "HNO_3 (1) pathway" due to the unconstrained isotope fractionation effect between HNO_3 and NO_3^-, resulting in the following equation:

$$\delta^{15}N\ (HNO_3)\ (1) = \delta^{15}N\ (NO_3^-)\ (1) \quad \text{(Eq. 1-3)}$$

O_3 pathways associated with N_2O_5, and NO_3.

During the nighttime when NO is oxidized into NO_2 without photolyzing back to NO, $\delta^{15}N\ (NO_2)$ should be reflective of the $\delta^{15}N$ of NO_x sources. If NO_2 is oxidized to N_2O_5, the isotopic equilibrium is likely to be achieved between NO_2, NO_3, and N_2O_5 by chemical equilibrium (R6) and the $\delta^{15}N$ values of N_2O_5 and NO_3 will reflect the equilibrium isotopic fractionation factors relative to NO_2 (i.e., $^{15}\alpha_{N2O5/NO2}$ and $^{15}\alpha_{NO3/NO2}$, values were adopted from Walters and Michalski (2016); supplementary Table S5). Finally, $\delta^{15}N$ of particulate NO_3^- produced from dark pathways can be expressed as the following (Walters and Michalski, 2016).

https://doi.org/10.5194/acp-2021-487
Preprint. Discussion started: 19 July 2021

Atmospheric Chemistry and Physics Discussions

207

208 $\delta^{15}N\ (HNO_3)\ (2) = \delta^{15}N\ (N_2O_5) = \delta^{15}N\ (NO_2) + \varepsilon_2$ (Eq. 2-1)

209 $\varepsilon_2 = 1000 \times ({}^{15}\alpha_{N2O5/NO2} - 1)$ (Eq. 2-2)

210 $\delta^{15}N\ (HNO_3)\ (2) = \delta^{15}N\ (NO_3^-)\ (2)$ (Eq. 2-3)

211 $\delta^{15}N\ (HNO_3)\ (3) = \delta^{15}N\ (NO_3) = \delta^{15}N\ (NO_2) + \varepsilon_3$ (Eq. 3-1)

212 $\varepsilon_3 = 1000 \times ({}^{15}\alpha_{NO3/NO2} - 1)$ (Eq. 3-2)

213 $\delta^{15}N\ (HNO_3)\ (3) = \delta^{15}N\ (NO_3^-)\ (3)$ (Eq. 3-3)

214

215 Therefore, the $\delta^{15}N\ (NO_x)$ in the atmosphere can be expressed using measured $\delta^{15}N\ (NO_3)$ and the net
216 N isotope fractionation effect, ε_N.

217 $\delta^{15}N\ (NO_2)_{atmosphere} = \delta^{15}N\ (NO_3^-)_{measured} - \varepsilon_N$ (Eq. 4-1)

218 $\varepsilon_N = \varepsilon_1 \times f_1 + \varepsilon_2 \times f_2 + \varepsilon_3 \times f_3$ (Eq. 4-2)

219 , where ε_1, ε_2, and ε_3 are abovementioned N isotope fractionation effect of pathways (i), (ii), and (iii),
220 respectively, and the proportional contributions (f_1, f_2, and f_3) of the three NO_3^- formation pathways
221 were estimated from $\Delta^{17}O$ measurements (Sect. 2.3.2).

222

223 **2.3.2. Proportional contributions of three formation pathways to atmospheric particulate**
224 **NO_3^-: $\Delta^{17}O\ (NO_3^-)$**

225 Due to its mass-independent nature, $\Delta^{17}O$ of particulate NO_3^- is a conservative tracer of
226 photochemical NO_3^- formation (Michalski et al., 2003), while $\delta^{15}N$ and $\delta^{18}O$ of NO_3^- can be significantly
227 modified by both equilibrium and kinetic isotope effects in the atmosphere (Elliott et al., 2019). At
228 photochemical steady state, the $\Delta^{17}O$ of NO_2 is determined by the relative production rate of NO_2 via
229 O_3 oxidation (R1) in NO_2 production (R1 and R2) (f_{O3}) and the mass-independent $\Delta^{17}O$ anomaly
230 transferred from O_3 during R1 ($\Delta^{17}O\text{-}O_3^*$):

231 $\Delta^{17}O\ (NO_2)\ (‰) = f_{O3} \times \Delta^{17}O\text{-}O_3^*$ (Eq. 5)

https://doi.org/10.5194/acp-2021-487
Preprint. Discussion started: 19 July 2021

Atmospheric Chemistry and Physics Discussions

f_{O3} was adopted from a previous study conducted in Beijing (Wang et al., 2019b), where the seasonal mean was 0.858 and 0.918 for summer and winter, respectively. $\Delta^{17}O\text{-}O_3^*$ can be approximated as 1.5 × $\Delta^{17}O\text{-}O_3$ because of the isotopic asymmetry of O_3 (Michalski and Bhattacharya, 2009). In this study, the $\Delta^{17}O\text{-}O_3^*$ is 37.5 ± 2.2‰ (mean ± SD) averaged from literature sources (Vicars et al., 2012; Vicars and Savarino, 2014).

The $\Delta^{17}O$ of particulate NO_3^- produced via the three formation pathways can be predicted by distinct $\Delta^{17}O$ transfer functions as the following (Morin et al., 2011):

$$\Delta^{17}O\ (NO_3^-)\ (1)\ (‰) = 2/3\ \Delta^{17}O(NO_2) = 2/3\ f_{O3} \times \Delta^{17}O\text{-}O_3^* \quad \text{(Eq. 6-1)}$$

$$\Delta^{17}O\ (NO_3^-)\ (2)\ (‰) = 5/6\ \Delta^{17}O(N_2O_5) = 1/3\ \Delta^{17}O(NO2) + 1/2\ \Delta^{17}O(NO_3) = 1/6\ \Delta^{17}O\text{-}O_3^*\ (4\ f_{O3} + 1) \quad \text{(Eq. 6-2)}$$

$$\Delta^{17}O\ (NO_3^-)\ (3)\ (‰) = \Delta^{17}O(NO_3) = 2/3\ \Delta^{17}O(NO_2) + 1/3\ \Delta^{17}O\text{-}O_3^* = 1/3\ \Delta^{17}O\text{-}O_3^*\ (2\ f_{O3} + 1) \quad \text{(Eq. 6-3)}$$

Finally, the $\Delta^{17}O\ (NO_3^-)$ can be expressed as the following:

$$\Delta^{17}O\ (NO_3^-)_{measured} = \Delta^{17}O\ (NO_3^-)\ (1) \times f_1 + \Delta^{17}O\ (NO_3^-)\ (2) \times f_2 + \Delta^{17}O\ (NO_3^-)\ (3) \times f_3 \quad \text{(Eq. 7)}$$

where $\Delta^{17}O\ (NO_3^-)_{measured}$ is the measured value in this study and the three endmember values of $\Delta^{17}O$ (NO_3^-) (1), $\Delta^{17}O\ (NO_3^-)$ (2), and $\Delta^{17}O\ (NO_3^-)$ (3) were calculated using Eqs. (6-1 to 6-3). The fractional contributions of the three NO_3^- formation pathways ($f_1 + f_2 + f_3 = 1$) were calculated by the SIAR model (Sect. 2.5.) for the winter and the summer months.

2.4. Estimation of $PM_{2.5}$ Aerosol Liquid Water (ALW) content and aerosol pH

ISORROPIA-II is a thermodynamic equilibrium model for the Cl^-, NO_3^-, SO_4^{2-}, Na^+, NH_4^+, K^+, Ca^{2+}, Mg^{2+}, and H_2O aerosol system (Fountoukis and Nenes, 2007). As input parameters, the concentrations of water-soluble ions and ambient RH and temperature were used for the model. In the present study, the model was run as a "forward" and "metastable" mode to calculate aerosol liquid water (ALW) content and pH. The detailed information of the model is found in Fountoukis and Nenes (2007).

https://doi.org/10.5194/acp-2021-487
Preprint. Discussion started: 19 July 2021


Atmospheric Chemistry and Physics Discussions

2.5. Bayesian stable isotope mixing model (SIAR; stable isotope analysis in R)

For source apportionment based on stable isotope composition, the Bayesian stable isotope mixing model (Parnell et al., 2013) was implemented using the SIMMR package in R software, which is available at https://cran.r-project.org/web/packages/simmr/index.html. The Bayesian Markov Chain Monte Carlo approach is adequate to provide the relative contribution of the sources. More information of the mixing model can be found in Parnell et al. (2010). The initial $\delta^{15}N$ of atmospheric NO_x was estimated from $\delta^{15}N$ (NO_3^-) for the source apportionment of NO_3^- particulates in $PM_{2.5}$ (Sect. 2.3.1). Then, the $\delta^{15}N$ (NO_x) of source endmembers were adopted from literature.

In addition, for quantifying proportional contribution of three NO_3^- formation pathways (f_1, f_2, and f_3 in Eq. 4-2), measured $\Delta^{17}O$ (NO_3^-) and $\Delta^{17}O$ (NO_3^-) endmember values of each pathway were treated in SIAR model.

2.6. Backward airmass trajectory

Two-day air mass backward trajectories were analyzed using the HYSPLIT (Hybrid Single-Particle Lagrangian Integrated Trajectory) model with meteorological input from the global data assimilation system (a regular 1° x 1° longitude-latitude grid) (Stein et al., 2015; https://ready.arl.noaa.gov/HYSPLIT.php) . The trajectories were calculated every 6 h at an elevation of 500 m above sea level. The potential source contribution function (PSCF) was then applied to calculate the probable source location (latitude i and longitude j), which is determined here as the ratio of the number of trajectory end points associated with measured $\delta^{15}N$ (NO_3^-) values higher than a threshold value (here, set to 95th percentile of $\delta^{15}N$ (NO_3^-) (m_{ij}) to the total number of points (n_{ij}) in the i j th grid cell. The PSCF calculation was made in the openair package, R software (https://cran.r-project.org/web/packages/openair/index.html) (Carslaw and Ropkins, 2012).

3. Results and discussion

3.1. Seasonal characteristics of $PM_{2.5}$, $\delta^{15}N$ (NO_3^-), and $\Delta^{17}O$ (NO_3^-)

$PM_{2.5}$ mass concentration varied from 7.5 μg m^{-3} to 139.0 μg m^{-3} for the whole sampling period.

https://doi.org/10.5194/acp-2021-487
Preprint. Discussion started: 19 July 2021


Atmospheric Chemistry and Physics Discussions

According to the typical synoptic weather patterns of East Asia (Kim et al., 2007), the measurements are divided into summer (May-Aug) and winter (Oct.-Mar.) groups. A clear seasonal difference in $PM_{2.5}$ concentration and its composition were observed with significantly higher concentrations of mass and inorganic constituent in the winter than in the summer (Table 1 and Figure S2).

During the summer, $PM_{2.5}$ concentration ranged from 7.5 μg m^{-3} to 34.5 μg m^{-3} with a mean of 22.0 ± 7.2 μg m^{-3}. The mean concentration of TC and TN was 4.6 ± 1.3 μgC m^{-3} and 1.9 ± 1.0 μgN m^{-3}, respectively, resulting in the mean TC/TN ratio of 2.8 ± 2.0. The mass concentrations of all measured species were much higher in the winter, during which $PM_{2.5}$ concentration was raised up to 139.0 μg m^{-3} from 10.6 μg m^{-3} with a mean of 61.7 ± 39.2 μg m^{-3}. Accordingly, the mean of TC and TN was 15.2 ± 4.5 μgC m^{-3} and 11.8 ± 7.7 μgN m^{-3}, respectively and the mean TC/TN ratio of 0.9 ± 0.7 was noticeably lower than that of the summer.

For the entire experiment, the mean mass fraction against $PM_{2.5}$ was the highest for NO_3^- (26% ± 23%), followed by SO_4^{2-} (20% ± 1%) and NH_4^+ (14% ± 1%), highlighting the contribution of SIA to $PM_{2.5}$ mass. The NO_3^- mass concentration varied from 0.2 μg m^{-3} to 69.3 μg m^{-3} with a mean of 17.0 ± 21.9 μg m^{-3}. In addition, the mass fraction of NO_3^- against TN were significantly higher in the winter (29.7 ± 22.1 μg m^{-3}; 38 %) than summer (0.8 ± 0.9 μg m^{-3}; 9%). The inorganic N from both NO_3^- and NH_4^+ dominated TN during the winter (TN = 0.97 × N from NO_3^- and NH_4^+ + 0.645). During the summer, NO_3^- and NH_4^+ comprised 68% of TN and the rest (32 %) was assumed to be organic nitrogen (ON) components. In contrast, the mass fraction of SO_4^{2-} against $PM_{2.5}$ was higher in the summer (23%) than winter (17%). The seasonal characteristics of chemical composition implies the significant role of inorganic nitrogen species in $PM_{2.5}$ mass increase in winter and ON and sulfate in summer.

The $\delta^{15}N$ (NO_3^-) exhibited higher values in winter with a weight-mean of -0.7‰ ± 3.3 ‰ and 3.8‰ ± 3.7 ‰ in the summer and the winter, respectively. Interestingly, the winter $\delta^{15}N$ (NO_3^-) values were overlapped with those observed in Beijing during late spring and between those of the two seasons in urban China, whereas the summer $\delta^{15}N$ (NO_3^-) fell in the range of those reported in urban China (Figure 1). The comparison of the measured $\delta^{15}N$ (NO_3^-) values, albeit very few, shows a clear seasonality in East Asia, which is mainly determined by synoptic meteorological condition that controls the type and strength of sources and atmospheric processing of pollutants transported after being emitted. Along with nitrogen isotope, heavier oxygen isotopes were also enriched in NO_3^- during the winter compared to the summer, when the weight-mean of $\delta^{17}O$, $\delta^{18}O$, and $\Delta^{17}O$ in NO_3^- were 70.4‰ ± 5.4 ‰, 82.0‰ ± 6.2 ‰, and 27.7‰ ± 2.2 ‰ for the winter and 57.3‰ ± 4.9 ‰, 65.7‰ ± 6.2 ‰, and 23.2‰ ± 2.2 ‰ for the

https://doi.org/10.5194/acp-2021-487
Preprint. Discussion started: 19 July 2021


Atmospheric Chemistry and Physics Discussions

summer.

As $PM_{2.5}$ concentrations reflect the seasonality, they were divided into 6 concentration bins from 0-20 μg m^{-3} to 100-140 μg m^{-3} considering the number of measurements, for which the chemical and meteorological properties were examined (Figure 2). For $PM_{2.5}$ greater than 40 μg m^{-3}, temperature stayed low with high relative humidity, representing the characteristics of high $PM_{2.5}$ episodes mostly in cold months. The concentrations of NO_3^-, SO_4^{2-}, and NH_4^+ linearly increased with $PM_{2.5}$ mass. Accordingly, the oxidation ratio of sulfur (SOR) and nitrogen (NOR) increased with $PM_{2.5}$, but gaseous precursors (NO_2 and SO_2) decreased in concentration at high $PM_{2.5}$ concentration greater than 40 μg m^{-3}. It is worthy of pointing that O_3 concentration was raised at high $PM_{2.5}$ concentration between 40 μg m^{-3} and 140 μg m^{-3}. Similarly, isotope ratios were correlated either linearly or inversely with $PM_{2.5}$ mass. $\Delta^{17}O$ (NO_3^-) showed the best correlation with $PM_{2.5}$ concentration like NO_3^-, whereas the dependence of $\delta^{15}N$ (NO_3^-) on $PM_{2.5}$ level was similar to those of precursor gases such as NO_2 and SO_2. In addition, the measured isotope ratios exhibited a good correlation with ambient temperature (Figure 1 and Figure S2). Of these, $\delta^{15}N$ (NO_3^-) was inversely correlated with temperature (r= -0.87) and a moderate correlation was found between $\Delta^{17}O$ (NO_3^-) and temperature (r= -0.55). These tendencies comprehensively indicate that the N and O isotope ratios are significantly affected by seasonally-varying sources, and substantially altered by equilibrium and kinetic isotope effects during the atmospheric processes.

3.2. Graphical representation of dual isotopes: $\delta^{15}N$ (NO_3^-) and $\Delta^{17}O$ (NO_3^-)

The isotope ratios of source endmembers are scarce in the study region and in the aerosol measurements, the isotope fractionation effect during gas-to-particle conversion is estimated with thermodynamic constants and reasonable assumptions. In this regard, the graphical representation of dual isotopes enables the complex signatures of atmospheric samples to be distinguished and allows their sources and processes to be constrained. Here, we introduce a plane with $\delta^{15}N$ (NO_3^-) and $\Delta^{17}O$ (NO_3^-) coordinates, where the ordered pairs correspond to the predicted $\delta^{15}N$ of NO_x source endmembers and $\Delta^{17}O$ (NO_3^-) endmembers of NO_3^- oxidation pathways. On the coordinates, the measured $\delta^{15}N$ (NO_3^-) and $\Delta^{17}O$ (NO_3^-) of each sample were displayed (Figure 3) (Rose et al., 2019). The domain of the three pathways is successfully distinguished, while $\delta^{15}N-\Delta^{17}O$ endmembers were calculated by allowing the key parameters to vary over a wide range.

https://doi.org/10.5194/acp-2021-487
Preprint. Discussion started: 19 July 2021


Atmospheric Chemistry and Physics Discussions

346 The $\delta^{15}N$ (NO_3^-) and $\Delta^{17}O$ (NO_3^-) values of all samples fell into the predicted ranges of the $\delta^{15}N-\Delta^{17}O$,
347 but were separated into seasonal groups (Figure 3). Most of summer $\Delta^{17}O$ (NO_3^-) values indicate OH
348 pathway (1), which is in accordance with what has been reported in temperate areas during summer
349 (Alexander et al., 2009; Michalski et al., 2003). Recently, the proportional contribution of the OH-
350 oxidation pathway was significantly correlated with latitudes in Chinese cities (Zong et al., 2020),
351 confirming the evidence of the NO_3^- formation through OH oxidation depending on UV radiation
352 intensity.

353 In comparison, more than half of winter samples are located in the domain indicating O_3 oxidation
354 pathways (2 & 3). When NO_3^- mass concentration was higher than ~ 3 μg m^{-3} in the summer and ~ 30
355 μg m^{-3} in the winter, $\Delta^{17}O$ (NO_3^-) values clearly represent the O_3 oxidation pathway (2). Despite the
356 short daytime and weak solar radiation intensity, the NO_3^- concentration was extremely high, leading to
357 severe haze pollution episodes in winter (Figure S2). This result suggests that the O_3 oxidation pathway
358 is likely to be responsible for the rapid conversion of particulate NO_3^-.

359 The formation of N_2O_5 (R6) is dependent on both NO_x and O_3, which are reciprocally correlated in
360 source regions. The equilibrium of R6 shifts to N_2O_5 at low temperature and its lifetime against
361 photolysis is long under the low sunlight. For these reasons, the dark formation of NO_3^- (R6) would be
362 favorable in urban outflows in winter. The hydrolysis of N_2O_5 on aerosol surface is highly dependent
363 on RH, aerosol liquid water content (AWLC), and chemical composition (Hallquist et al., 2003; Wahner
364 et al., 1998). In this section, we calculated the ALWC and acidity of aerosol, pH using ISORROPIA II
365 model and the measured concentrations of inorganic constituents in this study (Sect. 2.4.). Given the
366 high concentration of nano-particles from various sources in the urban areas, it is assured that aerosol
367 surface is enough for NO_3^- (2) pathway. During the entire experiment, RH was at the highest levels
368 when $PM_{2.5}$ mass was higher than 60 μg m^{-3} in the cold months (Figure 4a). The calculated ALWC was
369 higher by 90% (19.1 ± 22.8 μg m^{-3}) in the winter and lower by 21% (7.8 ± 5.2 μg m^{-3}) in the summer
370 relative to the annual mean of the two years. When NO_3^- mass concentrations were greater that ~ 3 μg
371 m^{-3} in summer and ~ 30 μg m^{-3} in winters, ALWC was 14.3 μg m^{-3} and 31.7 μg m^{-3}, respectively, which
372 were greater by 166% and 183% than the seasonal mean, respectively (Figure 4b). For the same
373 conditions, the aerosol pH remained almost the same during the summer (2.5) and lowered to 4.4
374 relative to the seasonal mean (4.7) during the winter. The lowered pH at the high $PM_{2.5}$ mass is
375 associated with sulfate formation and the high $PM_{2.5}$ mass was suggested to be the result of positive
376 feedback between hygroscopic inorganic salts and ALWC (Park, 2021). These findings support that
377 NO_3^- was efficiently converted from NO_x through the O_3 oxidation pathway (2), promoting the
378 development of $PM_{2.5}$ haze episode particularly in the cold months. In contrast, NO_3^- formation is

https://doi.org/10.5194/acp-2021-487
Preprint. Discussion started: 19 July 2021


Atmospheric Chemistry and Physics Discussions

attributed to the OH oxidation pathway (1) when $PM_{2.5}$ level was low in summer.

While $\Delta^{17}O$ (NO_3^-) allows the insights into the oxidation pathway of HNO_3, $\delta^{15}N$ (NO_3^-) values are affected by various factors, most of which are not well constrained due to the complicated chemistry and key roles of nitrogen oxides in the Earth's environment. In this study, $\delta^{15}N$ (NO_3^-) variability versus $PM_{2.5}$ concentration resembled the tendency of NO_2 (Figure 2), implying a close link between NO_2 oxidation and $\delta^{15}N$ (NO_3^-). Therefore, in addition to the role of $\Delta^{17}O$ (NO_3^-) as a tracer of HNO_3 oxidation pathway, we evaluated whether a variation of $\delta^{15}N$ (NO_3^-) indicates NO_x oxidation efficiency between NO and NO_2 (Freyer et al., 1993; Nelson et al., 2018; Walters et al., 2016).

In Seoul, NO and NO_2 mixing ratios are comparable (f_{NO2}= 0.4 to 0.8; Figure S3) with a mean NO_2 of 35.9 ± 14.4 ppbv for the experiment period. In this condition, $\delta^{15}N$ isotope effects should be driven by photochemical cycling (LCIE+EIE) (Freyer et al., 1993; Li et al., 2020). The $\delta^{15}N$ (NO_2) in the atmosphere will closely match the combined $\alpha_{NO2/NO}$ of EIE and LCIE for NO-NO_2 (Freyer et al., 1993; Li et al., 2020). However, a possible effect on $\delta^{15}N$ during NO_x photochemical cycling cannot be predicted in the same way under varying conditions, e.g., depending on abundances of NO, NO_2, and O_3. The shift in $\delta^{15}N$ (NO_2) relative to $\delta^{15}N$ (NO_x) in the atmosphere will change depending on f_{NO2} and temperature-dependent $\alpha_{NO2/NO}$(Freyer et al., 1993; Li et al., 2020; Walters et al., 2016). When O_3 mixing ratio is high, NO is almost completely oxidized to NO_2, leading to an increasing f_{NO2} value, and the $\delta^{15}N$ (NO_2) should correspond to the $\delta^{15}N$ of NO_x sources (Freyer et al., 1993).

In the dual isotope coordinates of $\delta^{15}N$ (NO_3^-) and $\Delta^{17}O$ (NO_3^-) (Figure 4), it is evident the samples taken during a record-breaking winter $PM_{2.5}$ pollution events are associated with the lower bound values of $\delta^{15}N$ (NO_3^-) (-1 to 4 ‰) and the highest $\Delta^{17}O$ (NO_3^-) values (28 to 31 ‰). The simultaneous measurements of PM_1 chemical composition in Seoul and Beijing demonstrated that the regionally-processed air masses were long-range transported to Seoul within approximately 2 days during these episodes (Kim et al., 2020a). Their NO_2/O_3 ratio (1 to 2) was clearly lower with higher f_{NO2} (0.7 to 0.8) compared to the other winter samples. This result implies that O_3 level was high enough to efficiently oxidize NO to NO_2 during the severe $PM_{2.5}$ pollution events. In this condition, the shift in $\delta^{15}N$ (NO_2) relative to $\delta^{15}N$ (NO_x) is insignificant and consequently, $\delta^{15}N$ (NO_2) would be lower than those of other winter samples unless both emission sources and $\alpha_{NO2/NO}$ changed significantly. Considering that NO_3^- is the key driver of the high $PM_{2.5}$ in Seoul, the higher degree of NO_x oxidation efficiency is worth highlighting, in conjunction with a strong linear relationship between $\Delta^{17}O$ (NO_3^-) and NOR (Figure 4e) revealing an efficient conversion of NO_2 to NO_3^- through O_3 oxidation pathway (2). The seasonally

https://doi.org/10.5194/acp-2021-487
Preprint. Discussion started: 19 July 2021


Atmospheric Chemistry and Physics Discussions

bifurcated $\delta^{15}N$ (NO_3^-) can be attributed primarily to the NO_x sources, which will be discussed in Section 3.4.

3.3. Contributions of major HNO_3 oxidation pathways

Combining the $\Delta^{17}O$ (NO_3^-) measurements and the calculation of $\Delta^{17}O$ transferred from O_3 to HNO_3, the contributions of three major NO_3^- formation pathways were quantitatively accounted, despite the inherent uncertainties in the calculation (Sect. 2.5.).

The OH oxidation (1) pathway dominated the total NO_3^- formation (87% ± 6%) in summer. In contrast, the nighttime pathways through N_2O_5 and NO_3 (pathways 2 and 3) were responsible for 24% and 14% of the NO_3^- formation in the winter, respectively. The contribution increased further to 40% and 30%, respectively, on haze days when $PM_{2.5}$ concentration exceeded 75 μg m^{-3}, national air quality standard for "very bad" alert.

The significant nighttime oxidation of NO_3^- has been observed broadly at urban sites in Northeast Asia. The results of this study are consistent with those conducted in Beijing, showing low $\Delta^{17}O$ values in summertime (about 17‰ to 25‰) and substantially high $\Delta^{17}O$ values (about 25‰ to 34‰) in wintertime when NO_3^--driven $PM_{2.5}$ haze pollution occurred (He et al., 2018; Song et al., 2020; Wang et al., 2019b). In general, nighttime pathways accounted for more than 60% and up to 97% in Beijing (He et al., 2018; Song et al., 2020; Wang et al., 2019b). Our summer and winter $\Delta^{17}O$ values are similar to those of annual ranges observed at an urban (Sapporo) and a rural (Rishiri) site in Japan, respectively (Nelson et al., 2018). It is also likely that the winter $\Delta^{17}O$ value in Seoul has undergone a considerable atmospheric processing on a regional scale. From a global perspective, the chemical transport model demonstrated that N_2O_5 heterogeneous hydrolysis was comparably important as NO_2 +OH (41 %) for NO_3^- formation at below 1km altitude (Alexander et al., 2020).

It is noteworthy that although the seasonal patterns are similar in Northeast Asia, the average proportional contributions estimated from $\Delta^{17}O$ (NO_3^-) are highly sensitive to input parameters (i.e, f_{O3} and $\Delta^{17}O\text{-}O_3$*). In this study, the seasonal f_{O3} was assumed to be equal to those estimated for Beijing and set to 0.858 ± 0.05 and 0.918 ± 0.05 for the warm and cold months, respectively (Wang et al., 2019b), which are comparable to other estimates for Beijing (0.86) and Shanghai (0.97) (He et al., 2018, 2020) and the annual-mean of 0.85 in a global model (Alexander et al., 2020).

The uncertainty associated with $\Delta^{17}O\text{-}O_3$* has been recognized as the largest source of uncertainty in

https://doi.org/10.5194/acp-2021-487
Preprint. Discussion started: 19 July 2021

Atmospheric Chemistry and Physics Discussions

estimating NO_3^- production pathways from $\Delta^{17}O$ (NO_3^-) (Alexander et al., 2009, 2020). In this study, the $\Delta^{17}O$-O_3* of 37.5‰ ± 2.2‰ was averaged from previous observations, corresponding to $\Delta^{17}O$-bulk O_3 of 25‰ (Vicars et al., 2012; Vicars and Savarino, 2014). Our mean $\Delta^{17}O$-O_3* of 37.5‰ was 2.8‰ higher and 1.5‰ lower than what was used in (Liu et al., 2020; Wang et al., 2019b) and (He et al., 2018, 2020) for urban Beijing and Shanghai, respectively. When sensitivity test was conducted for the proportional contribution of the three oxidation pathways, a 2.8‰ change in $\Delta^{17}O$-O_3* value caused 1.6‰, 2.1‰, and 2.5‰ change in the endmember for (1), (2), and (3) pathway, respectively. As a result, the average contribution of the nighttime pathways, including NO_3^- (2) and NO_3^- (3), increased to 23 % in summer and 65 % in winter. This suggests that a proper use of key parameters driving endmember values is pre-requisite for more realistic quantification of NO_3^- oxidation pathway contributions.

3.4. Quantifying relative contribution of major NO_x sources

In Seoul, the seasonal trend of $\delta^{15}N$ (NO_3^-) was distinct with lower and higher values in the summer and the winter, respectively. In particular, the lower and the upper bound of $\delta^{15}N$ (NO_3^-) were associated with air masses from the ocean by southerly and easterly in the summer and from Siberia by northerly in winter, respectively (Figure S4). This seasonal pattern of $\delta^{15}N$ (NO_3^-) has been typically observed in Northeast Asia regions, which is affected by monsoon system (Li et al., 2019; Song et al., 2019; Zong et al., 2020). Meanwhile, at a mountain station in Taiwan, the highest $\delta^{15}N$ (NO_3^-) was found in spring when the level of anthropogenic constituents were elevated (Guha et al., 2017). These observations over East Asia suggest that the seasonal difference in $\delta^{15}N$ (NO_3^-) mainly reflects the emission sources, where low and high $\delta^{15}N$ (NO_3^-) values indicate biogenic soil emissions and coal combustion respectively (Elliott et al., 2019).

In comparison with $\delta^{15}N$ (NO_3^-) values in urban China (Song et al., 2019; Zong et al., 2020), the summer values in Seoul (-0.7‰ ± 2.6‰) are quite similar to those in Beijing and Shanghai (~ 0‰ to 2‰), whereas winter values (3.8‰ ± 3.7‰; arithmetic mean 6.4‰ ± 3.8‰) are noticeably lower in Seoul than in other Chinese cities (~ 6‰ to 14‰). It implies that the source variability would cause the large difference in winter $\delta^{15}N$ (NO_3^-) values between the two sites. The $\delta^{15}N$ (NO_3^-) studies in urban China have reported coal combustion as the highest contribution source to atmospheric NO_x emissions during winter, about 30% to 40 %, regardless approaches used for estimating NO_3^- oxidation pathway, either $\Delta^{17}O$ or $\delta^{18}O$ (Li et al., 2019; Song et al., 2019, 2020; Zong et al., 2020).

To investigate major emission sources of atmospheric NOx in Seoul, we simulated the proportional

https://doi.org/10.5194/acp-2021-487
Preprint. Discussion started: 19 July 2021

Atmospheric Chemistry and Physics Discussions

471 contributions of NO_x emission sources to the NO_3^- of $PM_{2.5}$, based on $\delta^{15}N$ (NO_2) estimated from $\delta^{15}N$
472 (NO_3^-) with considering nitrogen isotopic fractionation effects, $\delta^{15}N$ (NO_2- NO_3^-), using dual isotopes
473 ($\Delta^{17}O$ and $\delta^{15}N$) and $\delta^{15}N$ end-member values of major NO_x sources (Sect. 2.3.). The estimated ε_N values
474 were 4.0‰ ± 0.6‰ and 10.2‰ ± 0.7‰, and accordingly the $\delta^{15}N$ $(NO_2)_{atmosphere}$ was -6.7‰ ± 2.9‰ and
475 -3.5‰ ± 3.9‰ in summer and winter, respectively.

476 The $\delta^{15}N$ (NO_x) endmember values were adopted from literature; biogenic soil (driven by fertilizer use;
477 -35.1‰ ± 10.2‰) (Felix and Elliott, 2014; Li and Wang, 2008; Yu and Elliott, 2017), biomass burning
478 (1.8‰ ± 1.8‰) (Fibiger and Hastings, 2016), vehicle emissions (-2.5‰ ± 1.5‰) (Walters et al., 2015),
479 and coal combustion (14.2‰ ± 4.5‰) (Felix et al., 2012; Heaton, 1990). Clearly, the estimated source
480 contributions were different between with and without isotope fractionation effects for conversion of
481 NO_x to NO_3^- (Figure 5a and b). As a result, the vehicle emission was the largest source contributor with
482 34% and 31% in summer and winter, respectively (Figure 5c and Figure S5). The relative contribution
483 of the major NO_x sources in Seoul is given in order as the following:

484 Summer: vehicle emissions > biomass burning > biogenic soil >coal combustion

485 Winter: vehicle emissions > biomass burning > coal combustion > biogenic soil

486 This result is partly supported by a better correlation of NO_2 with CO than with SO_2 for both seasons.
487 According to an (anthropogenic) emission inventory (CAPSS, 2016), total mobile sources account for
488 about two-third of NO_x emissions in Korea, followed by combustion sources such as energy and
489 manufacturing industries (33%). The highest NO_2 column densities are distinct in Seoul Metropolitan
490 Areas (SMA), which is mostly due to the emissions from transportation (Kim et al., 2020b). Our results
491 of the isotope measurements are in fairly good agreement with the national emission inventories and
492 satellite observations, indicating the largest contribution of vehicle emissions to NO_x sources in Seoul.
493 Other than vehicle emissions, the contribution of fertilized soil emissions was higher during the summer,
494 whereas emissions from coal combustion was larger during the winter. The seasonally distinct
495 contribution of these emission sources was consistent with the results from previous studies conducted
496 in China, revealing common seasonal sources on a regional scale in East Asia.

497 It was evident in several winter samples that the mass ratio of SO_4^{2-}/ NO_3^- was 2~3 times higher with
498 the highest $\delta^{15}N$ (NO_3^-) values (>10‰) comparable to the NO_x endmember values of coal combustion
499 (Elliott et al., 2019). They are also similar to the winter $\delta^{15}N$ (NO_3^-) values of urban China (Zong et al.,
500 2020). The increased contribution of coal in winter was primarily attributed to emissions from industries
501 or residential heating in northern China. During this period, trajectory analysis indicates that air masses

https://doi.org/10.5194/acp-2021-487
Preprint. Discussion started: 19 July 2021


Atmospheric Chemistry and Physics Discussions

originated from cold regions in northeastern China, such as Liaoning province, where heavy and coal-fired industries are located.

However, the relative contribution of biomass burning was greater than that of coal combustion in the winter as well as in the summer. It implies that the study region is under influence of various biomass burning sources throughout a year, such as agricultural combustion in vicinities of Seoul and over eastern China from spring to fall (Chen et al., 2017; Zhao et al., 2017), wild fires over Siberia and Russian Far East in summer (van der Werf et al., 2010), and residential biomass combustion for heating over east Asia in winter. This finding of our isotope-based study highlights the substantial role of biomass combustion in northeast Asia from local to regional scale, which was not realistically considered in emission inventories that mostly focus on anthropogenic sources.

In this study, it is particularly noteworthy that the lower winter $\delta^{15}N$ (NO_3^-) and thus relatively lower contribution of coal combustion confirms the recent trend that emissions from coal combustion have been reduced in China (Cheng et al., 2019; Tong et al., 2018). Our study was conducted in later years (2018-2019) than their studies (2013-2017), of which $\delta^{15}N$ (NO_3^-) values were rather comparable to the winter mean $\delta^{15}N$ (NO_3^-) observed in Seoul during January 2014 ~ February 2016 (11.9‰ ± 2.5‰; Park et al., 2018). The lower bound of winter $\delta^{15}N$ (NO_3^-) values associated with the highest NO_3^- and $PM_{2.5}$ concentrations (Figures 3 and 4) was considered a result of complex effects of isotopic fractionation, as discussed above.

4. Conclusions

Our stable isotope-based study confirms that vehicle emissions are the main source of NO_3^- in $PM_{2.5}$ in Seoul throughout the year. In addition, the contribution of biomass combustion from various activities was found to be substantial than estimated by bottom-up emission inventories. While emission sources of NO_x were not variable seasonally, the contribution of coal combustion and biogenic soil emissions were slightly enhanced in winter and summer, respectively. Given that severe winter haze events with daily $PM_{2.5}$ exceeding 100 μg m^{-3} were mainly driven by NO_3^- (up to ~60 % in $PM_{2.5}$), reduction in NO_x emissions from vehicles is essential for an effective mitigation measure to improve fine aerosol pollution in the study region. Particularly, the highest $PM_{2.5}$ was concurrent with the highest NOR and $\Delta^{17}O$ (NO_3^-), and the lowest $\delta^{15}N$ (NO_3^-), revealing the heterogeneous conversion of particulate NO_3^- through O_3 oxidation during the winter haze episodes. The multiple-isotope signatures of particulate NO_3^-, including ^{17}O, ^{18}O, and ^{15}N, highlights the secondary nature of fine aerosol pollution intimately

https://doi.org/10.5194/acp-2021-487
Preprint. Discussion started: 19 July 2021


Atmospheric Chemistry and Physics Discussions

coupled with the photochemical oxidation process and allows a quantitative understanding of distinct oxidation processes as well as the attribution of NO_x sources. Further studies of multiple isotopes for multiple phases will help to elucidate the detailed mechanism of gas-to-particle conversion and transformation leading to severe haze development.

Acknowledgement

This research was supported by the National Strategic Project-Fine Particle of the National Research Foundation of Korea (NRF), funded by the Ministry of Science and ICT (MSIT), Ministry of Environment (ME), and Ministry of Health and Welfare (MOHW) (2017M3D8A1092015). Funding to S. Lim was provided by the National Research Foundation of Korea (NRF) from the Ministry of Science and ICT (2018R1D1A1B07050849). M. Lee thanks for the support from NRF (2020R1A2C3014592). J. Savarino thanks the French National Research Agency (Investissements d'avenir grant ANR-15-IDEX-02) and the INSU programme LEFE-CHAT for supporting the stable isotope laboratory. This is publication 4 of PANDA platform on which isotope analyses were performed.

https://doi.org/10.5194/acp-2021-487
Preprint. Discussion started: 19 July 2021

Atmospheric Chemistry and Physics Discussions

549 **Table and figures**

550 **Tables**

551

552 **Table 1. Measurement summary of $PM_{2.5}$ chemical constituents and isotopic composition in Seoul**
553 **during the sampling period of May. 2018-Mar. 2019. Arithmetic mean ± 1 standard**
554 **deviation (mass fraction, %) for mass concentration and concentration-weight mean ± 1**
555 **standard deviation for isotope ratios.**

556

Constituents	Summer (n=14)	Winter (n=18)
$PM_{2.5}$ (μg m^{-3})	22.0±7.2	71.22 ± 29.01
TC	4.6±1.3 (21%)	15.2±4.5 (21%)
TN	1.9±1.0 (9%)	11.8±7.7 (54%)
NO_3^-	0.8±0.9 (4%)	29.7±22.1 (42%)
NH_4^+	1.79 ± 0.76 (8%)	11.7 ± 8.4 (16%)
SO_4^{2-}	5.2 ± 2.2 (23%)	11.5 ± 9.2 (16%)
$[NH_4^+]/([SO_4^{2-}]+[NO_3^-])$ equiv. ratio	0.84 ± 0.07	0.94 ± 0.09
$\delta^{15}N$ (NO_3^-)	-0.7±3.3	3.8±3.7
$\delta^{17}O$	57.3±4.9	70.4±5.4
$\delta^{18}O$	65.7±6.2	82.0±6.2
$\Delta^{17}O$	23.2±2.2	27.7±2.2

557

558

https://doi.org/10.5194/acp-2021-487
Preprint. Discussion started: 19 July 2021

Atmospheric Chemistry and Physics Discussions

559 **Figures.**

560

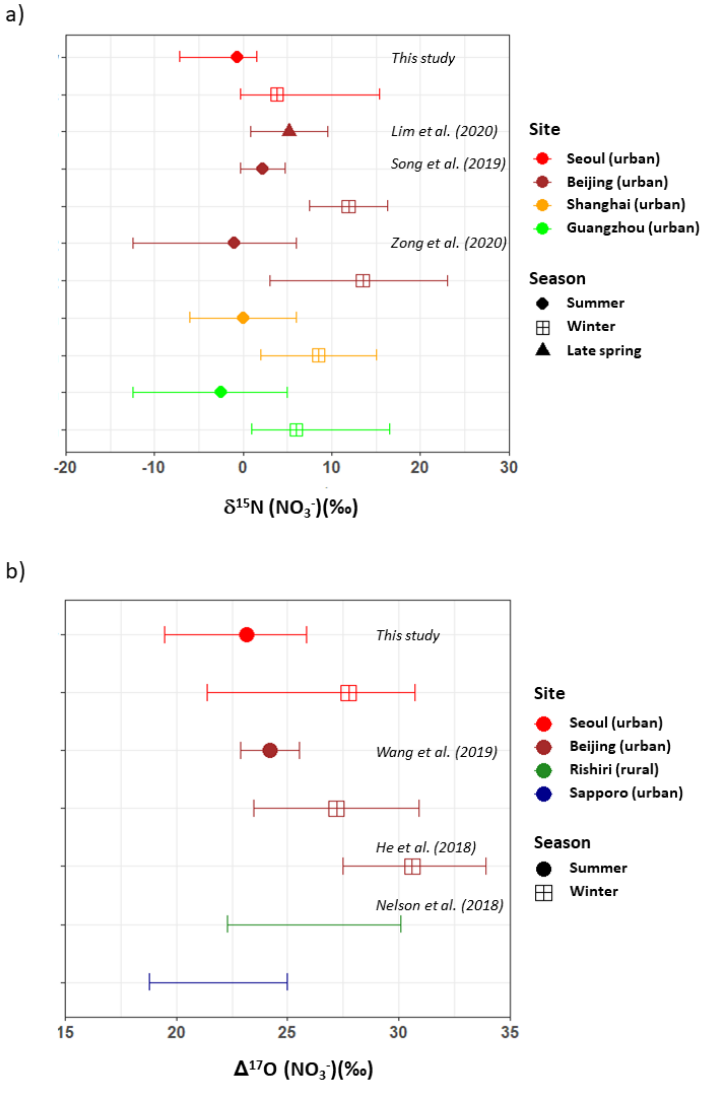

561

562

563 **Figure 1. Ranges of $\delta^{15}N$ (NO_3^-) and $\Delta^{17}O$ (NO_3^-) of $PM_{2.5}$ in Northeast Asia. (a) Ranges of $\delta^{15}N$**
564 **(NO_3^-). (b) Ranges of $\Delta^{17}O$ (NO_3^-). Different colors denote sites; Seoul in this study in**
565 **red, Beijing, Shanghai, and Guangzhou in China in brown, orange, light green,**

https://doi.org/10.5194/acp-2021-487
Preprint. Discussion started: 19 July 2021

Atmospheric Chemistry and Physics Discussions

566 **respectively, and Rishiri and Sapporo in Japan in green and blue, respectively. Different**
567 **marker shapes denote seasons. Points indicates mean value (concentration-weighted**
568 **average for Seoul samples in this study) and lower and upper whiskers denote min and**
569 **maximum values (This study; He et al., 2018; Lim et al., 2020; Nelson et al., 2018), ±**
570 **standard deviation (Song et al., 2019; Wang et al., 2019b), or 25th and 75th percentiles**
571 **(Zong et al., 2020).**

572

573

a)

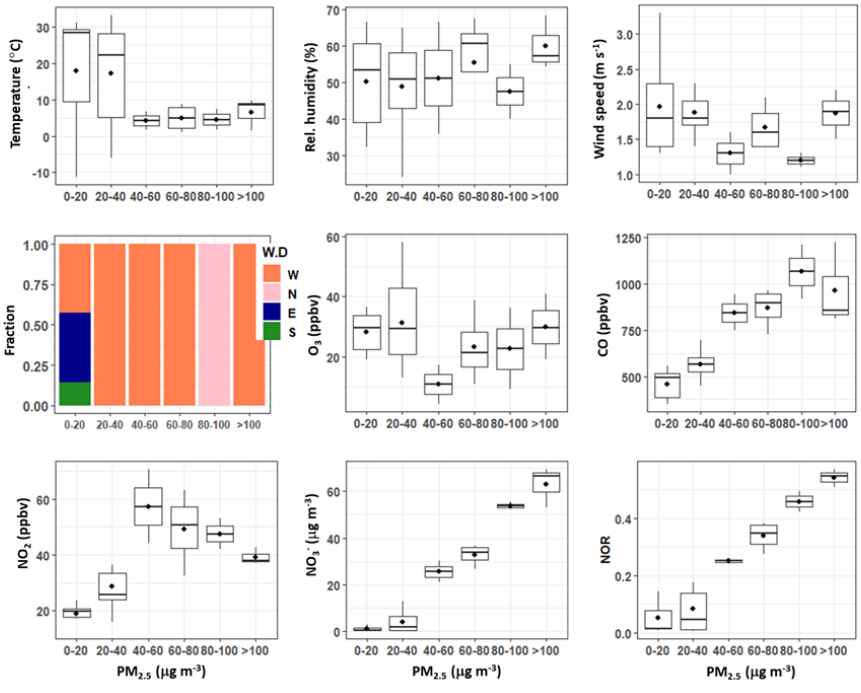

574

https://doi.org/10.5194/acp-2021-487
Preprint. Discussion started: 19 July 2021

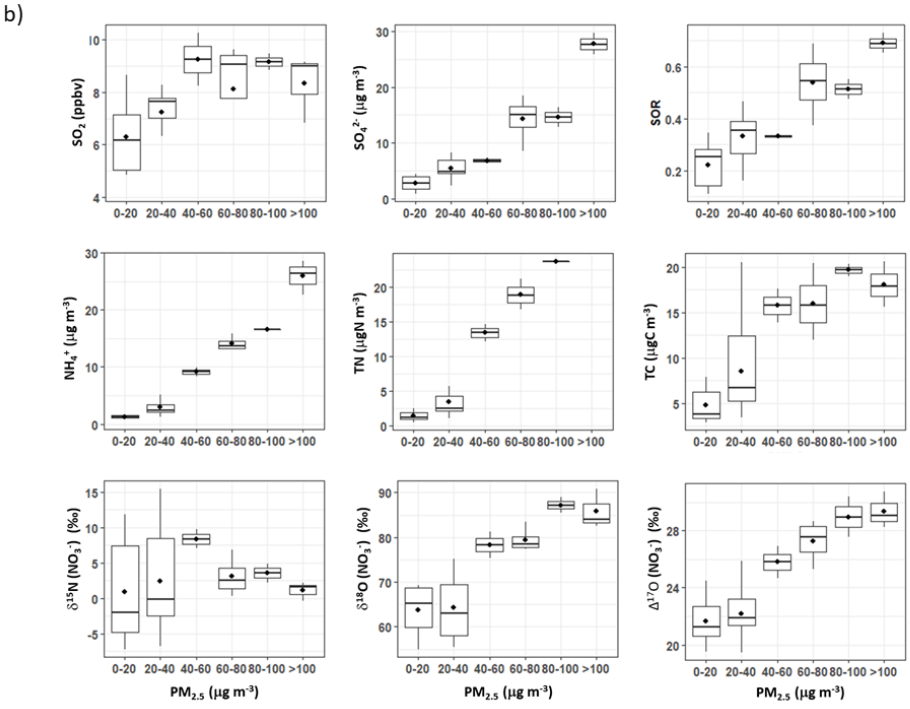

Figure 2. Box-whisker plots as a function of $PM_{2.5}$ mass concentration in Seoul for the sampling period.

https://doi.org/10.5194/acp-2021-487
Preprint. Discussion started: 19 July 2021

Atmospheric Chemistry and Physics Discussions

a)

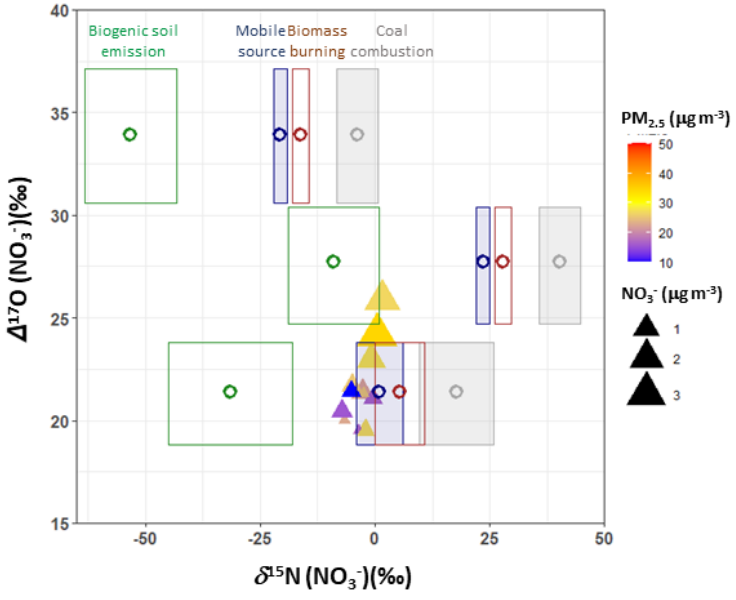

578

b)

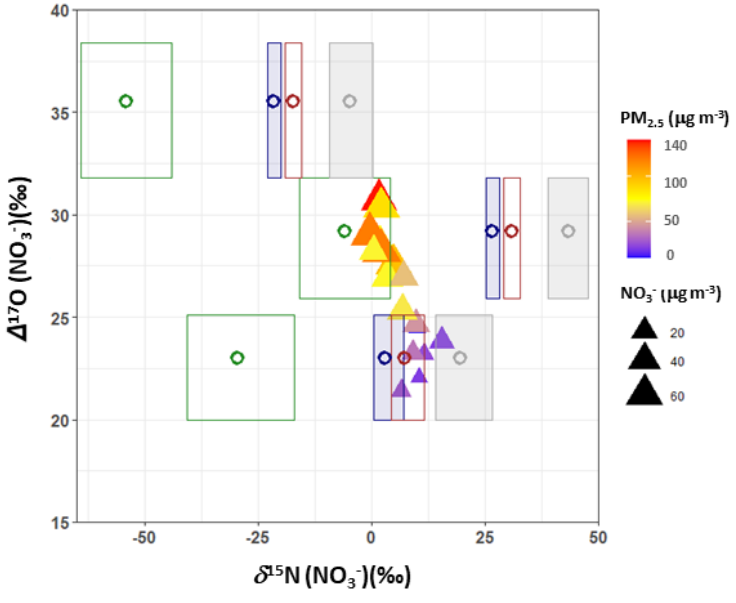

579

https://doi.org/10.5194/acp-2021-487
Preprint. Discussion started: 19 July 2021

Atmospheric Chemistry and Physics Discussions

580 **Figure 3. Measured $\delta^{15}N$ (NO_3^-) and $\Delta^{17}O$ (NO_3^-) values (closed triangles) compared to the**
581 **predicted $\delta^{15}N$ (NO_3^-) and $\Delta^{17}O$ (NO_3^-) compositions for the tree major NO_3^- formation**
582 **pathways (open circles) in (a) summer and (b) winter. Colors of open circles indicate**
583 **different source endmembers (biogenic soil emission in green, mobile source in navy,**
584 **biomass burning in brown, and coal combustion in grey), assuming seasonal mean f_{NO2}**
585 **of 0.8 and 0.69 for summer and winter, respectively, and $\Delta^{17}O$ (O_3*) of 37.5 ± 2.2 ‰.**
586 **Shaded rectangles denote the range of $\delta^{15}N$ (NO_3^-) and $\Delta^{17}O$ (NO_3^-) compositions**
587 **calculated considering propagation of uncertainties in $\delta^{15}N$ of NO_x source endmembers,**
588 **f_{NO2}, f_{O3}, and $\Delta^{17}O$ (O_3*). Marker size and color of measured values indicate NO_3^-**
589 **concentration and $PM_{2.5}$ concentration, respectively.**

590

591

592 a)

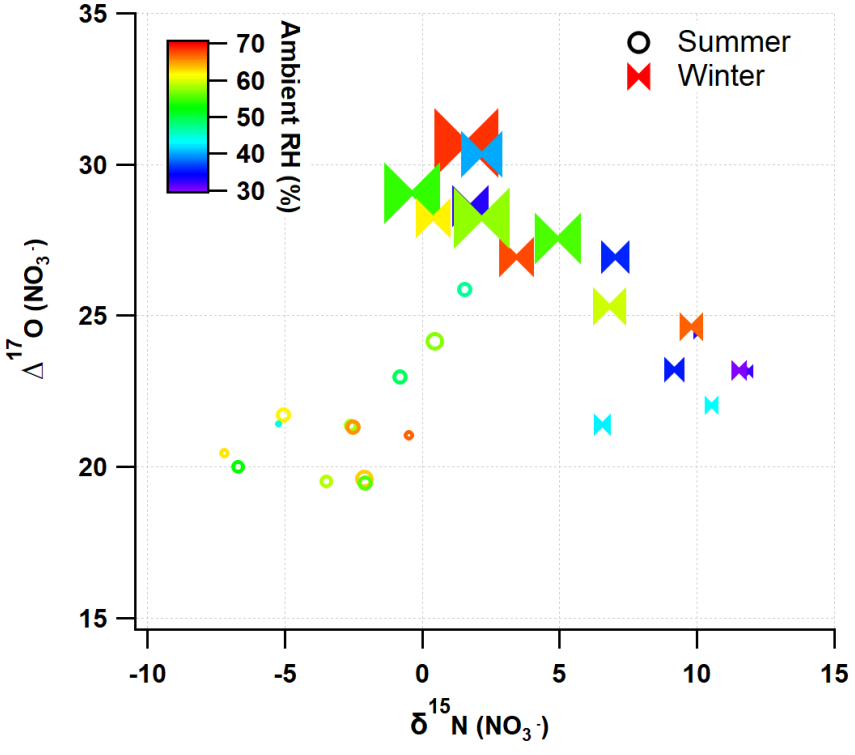

593

https://doi.org/10.5194/acp-2021-487
Preprint. Discussion started: 19 July 2021

Atmospheric Chemistry and Physics Discussions

b)

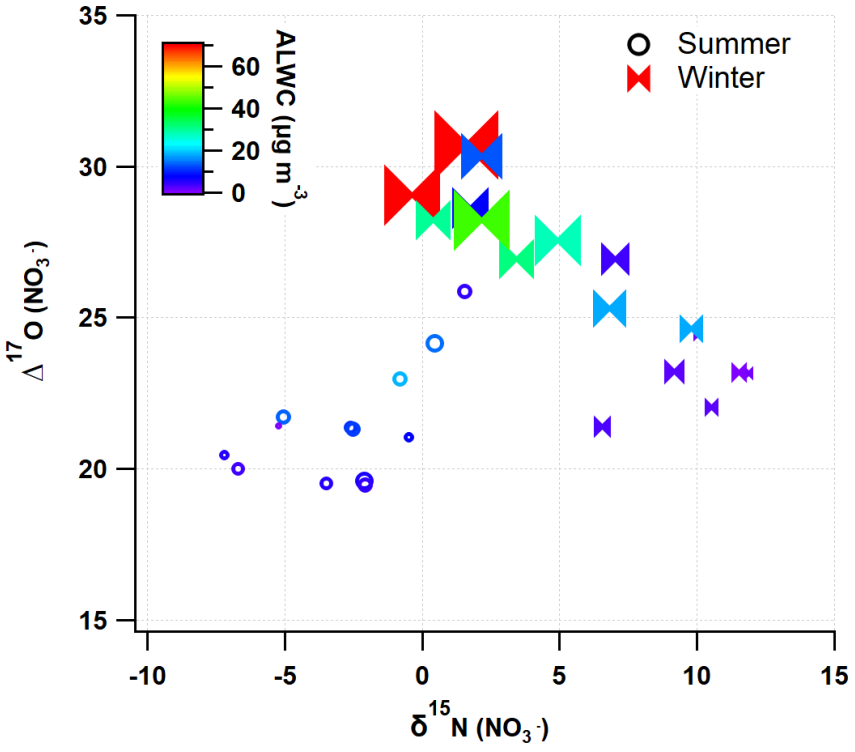

https://doi.org/10.5194/acp-2021-487
Preprint. Discussion started: 19 July 2021

Atmospheric Chemistry and Physics Discussions

597 c)

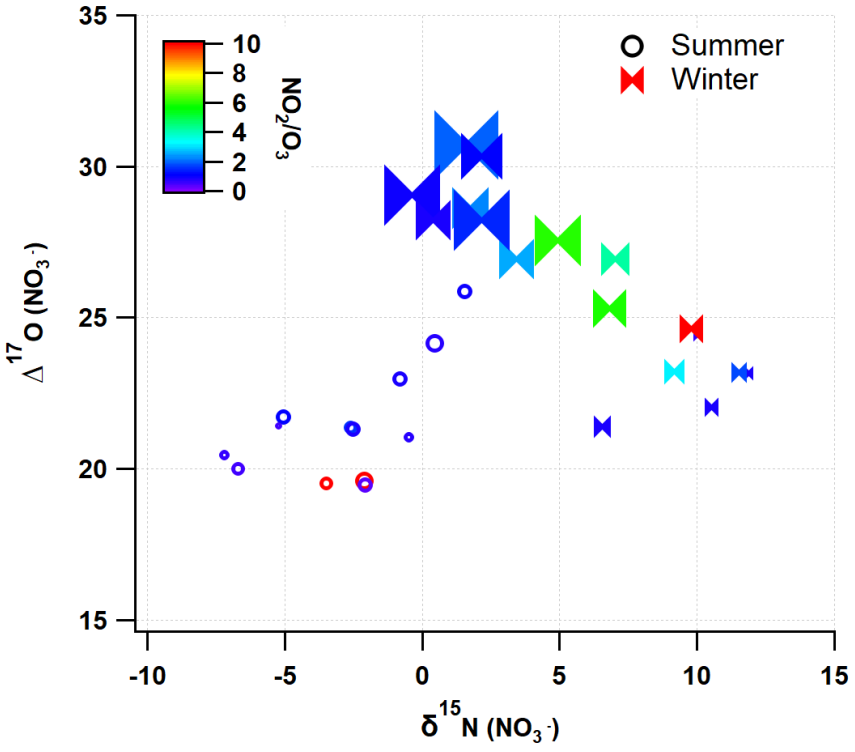

598

599

https://doi.org/10.5194/acp-2021-487
Preprint. Discussion started: 19 July 2021

Atmospheric Chemistry and Physics Discussions

600 d)

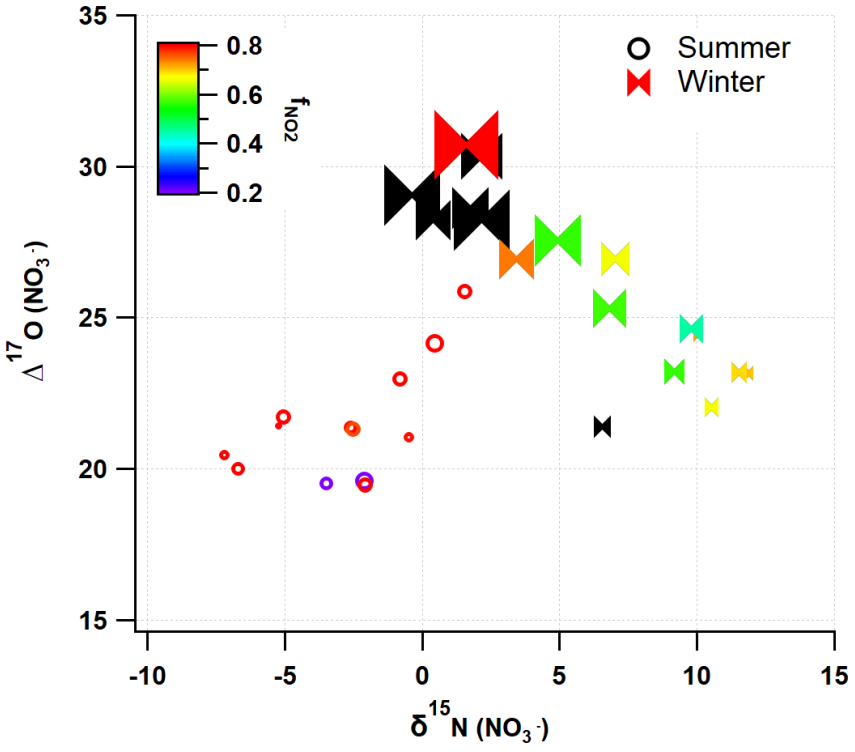

601

602

https://doi.org/10.5194/acp-2021-487
Preprint. Discussion started: 19 July 2021

Atmospheric Chemistry and Physics Discussions

603 e)

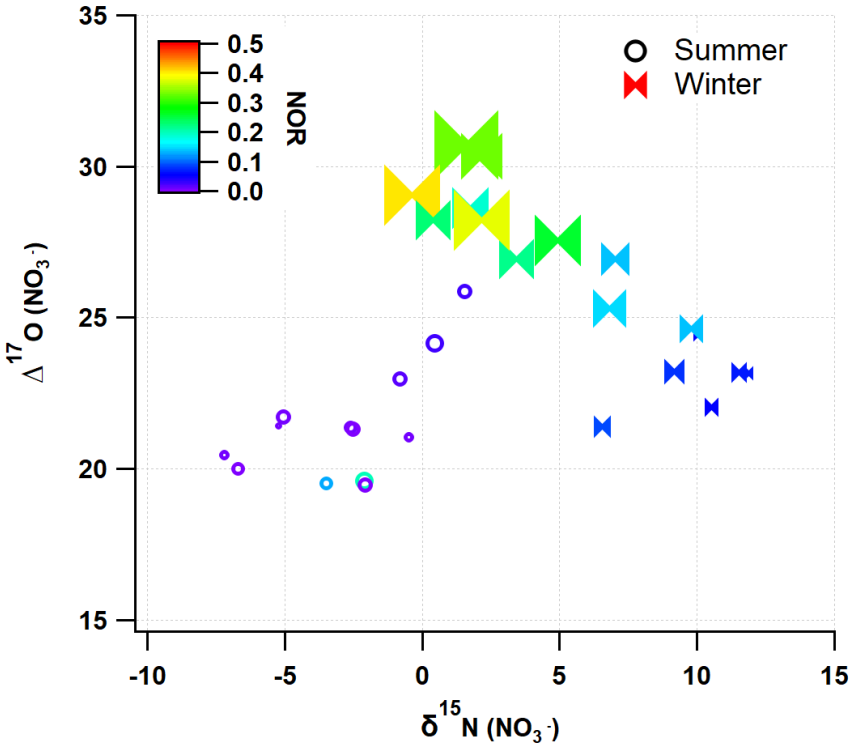

604

605

https://doi.org/10.5194/acp-2021-487
Preprint. Discussion started: 19 July 2021

Atmospheric Chemistry and Physics Discussions

606 f)

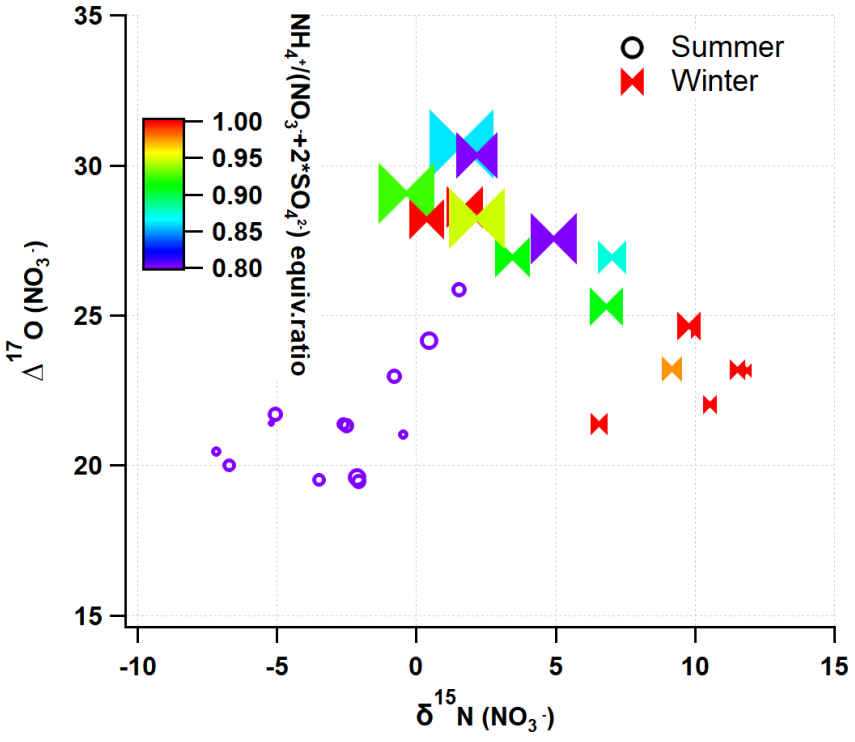

607

608 **Figure 4. Measured $\delta^{15}N$ (NO_3^-) and $\Delta^{17}O$ (NO_3^-) values with associated parameters including (a)**
609 **ambient RH, (b) ALWC, (c) NO_2/O_3 ratio, (d) f_{NO2}, (e) NOR, and (f)**
610 **$[NH_4^+]/([SO_4^{2-}]+[NO_3^-])$ equivalent ratio.**

611

612

https://doi.org/10.5194/acp-2021-487
Preprint. Discussion started: 19 July 2021

Atmospheric Chemistry and Physics Discussions

613 a)

614

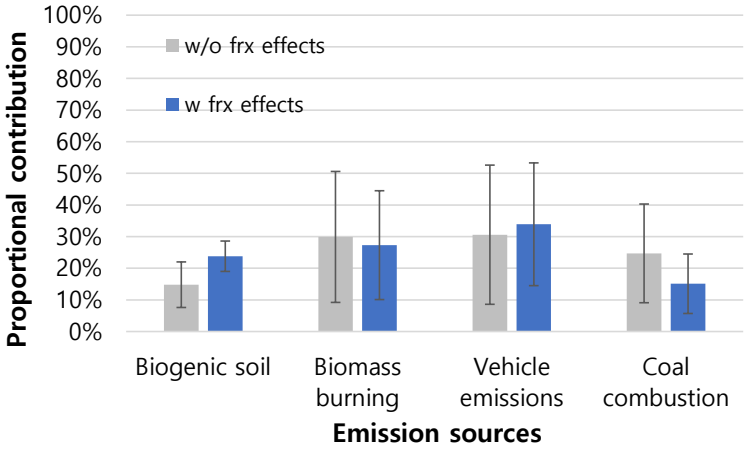

615

616 b)

617

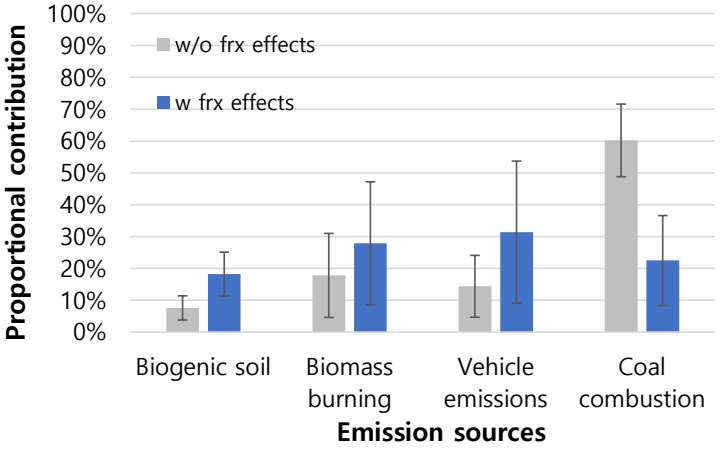

618

619

https://doi.org/10.5194/acp-2021-487
Preprint. Discussion started: 19 July 2021

Atmospheric Chemistry and Physics Discussions

620 c)

621

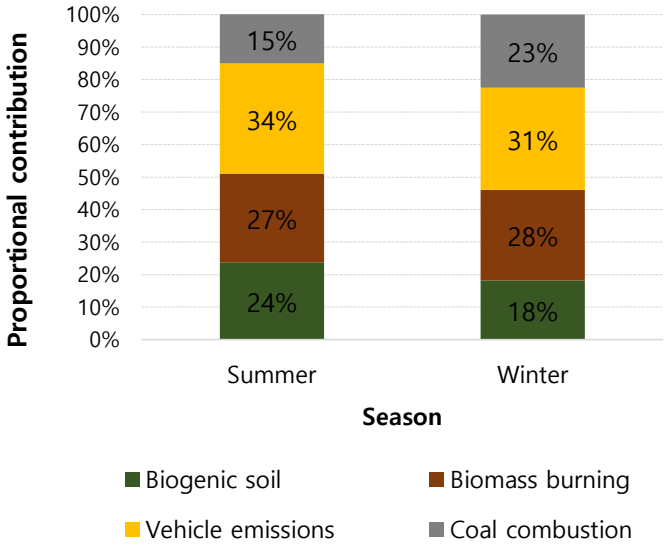

622

623 **Figure 5. Seasonal proportional contribution of major NO_x emission sources to NO_3^- of $PM_{2.5}$ in**
624 **Seoul. Comparison of simulation results with and without including isotope**
625 **fractionation effects in the Bayesian model calculations in (a) summer and (b) winter. (c)**
626 **Best estimates for summer and winter.**

627

https://doi.org/10.5194/acp-2021-487
Preprint. Discussion started: 19 July 2021

Atmospheric Chemistry and Physics Discussions

628 **References**

629 Alexander, B., Hastings, M. G., Allman, D. J., Dachs, J., Thornton, J. A. and Kunasek, S. A.:
630 Quantifying atmospheric nitrate formation pathways based on a global model of the oxygen isotopic
631 composition (Δ¹⁷O) of atmospheric nitrate, Atmos. Chem. Phys.,
632 9(14), 5043–5056, doi:10.5194/acp-9-5043-2009, 2009.

633 Alexander, B., Sherwen, T., Holmes, C. D., Fisher, J. A., Chen, Q., Evans, M. J. and Kasibhatla, P.:
634 Global inorganic nitrate production mechanisms: comparison of a global model with nitrate isotope
635 observations, Atmos. Chem. Phys., 20(6), 3859–3877, doi:10.5194/acp-20-3859-2020, 2020.

636 Carslaw, D. C. and Ropkins, K.: openair — An R package for air quality data analysis, Environ.
637 Model. Softw., 27–28, 52–61, doi:10.1016/j.envsoft.2011.09.008, 2012.

638 Casciotti, K. L., Sigman, D. M., Hastings, M. G., Böhlke, J. K. and Hilkert, A.: Measurement of the
639 oxygen isotopic composition of nitrate in seawater and freshwater using the denitrifier method, Anal.
640 Chem., 74(19), 4905–4912, doi:10.1021/ac020113w, 2002.

641 Chang, Y., Zhang, Y., Tian, C., Zhang, S., Ma, X., Cao, F., Liu, X., Zhang, W., Kuhn, T. and
642 Lehmann, M. F.: Nitrogen isotope fractionation during gas-to-particle conversion of NOx to NO3- in
643 the atmosphere– implications for isotope-based NOx source apportionment, Atmos. Chem. Phys.,
644 18(16), 11647–11661, doi:10.5194/acp-18-11647-2018, 2018.

645 Chen, J., Li, C., Ristovski, Z., Milic, A., Gu, Y., Islam, M. S., Wang, S., Hao, J., Zhang, H., He, C.,
646 Guo, H., Fu, H., Miljevic, B., Morawska, L., Thai, P., LAM, Y. F., Pereira, G., Ding, A., Huang, X.
647 and Dumka, U. C.: A review of biomass burning: Emissions and impacts on air quality, health and
648 climate in China, Sci. Total Environ., 579(November 2016), 1000–1034,
649 doi:10.1016/j.scitotenv.2016.11.025, 2017.

650 Cheng, J., Su, J., Cui, T., Li, X., Dong, X., Sun, F., Yang, Y., Tong, D., Zheng, Y., Li, J., Zhang, Q.
651 and He, K.: Dominant role of emission reduction in PM2.5 air quality improvement in Beijing during
652 2013-2017: a model-based decomposition analysis, Atmos. Chem. Phys., 19(Cheng, J., Su, J., Cui, T.,
653 Li, X., Dong, X., Sun, F., Yang, Y., Tong, D., Zheng, Y., Li, J., Zhang, Q., He, K., 2019. Dominant
654 role of emission reduction in PM2.5 air quality improvement in Beijing during 2013-2017: a model-
655 based decomposition analysis.), 6125–6146, doi:10.5194/acp-19-6125-2019, 2019.

656 Elliott, E. M., Yu, Z., Cole, A. S. and Coughlin, J. G.: Isotopic advances in understanding reactive

https://doi.org/10.5194/acp-2021-487
Preprint. Discussion started: 19 July 2021


Atmospheric Chemistry and Physics Discussions

657 nitrogen deposition and atmospheric processing, Sci. Total Environ., 662, 393–403,
658 doi:10.1016/J.SCITOTENV.2018.12.177, 2019.

659 Felix, J. D. and Elliott, E. M.: Isotopic composition of passively collected nitrogen dioxide emissions:
660 Vehicle, soil and livestock source signatures, Atmos. Environ., 92, 359–366,
661 doi:10.1016/j.atmosenv.2014.04.005, 2014.

662 Felix, J. D., Elliott, E. M. and Shaw, S. L.: Nitrogen Isotopic Composition of Coal-Fired Power Plant
663 NO x : Influence of Emission Controls and Implications for Global Emission Inventories, Environ.
664 Sci. Technol., 46(6), 3528–3535, doi:10.1021/es203355v, 2012.

665 Fibiger, D. L. and Hastings, M. G.: First Measurements of the Nitrogen Isotopic Composition of NO
666 $_x$ from Biomass Burning, Environ. Sci. Technol., 50(21), 11569–11574,
667 doi:10.1021/acs.est.6b03510, 2016.

668 Fountoukis, C. and Nenes, A.: ISORROPIA II: a computationally efficient thermodynamic
669 equilibrium model for K+- Ca2+-Mg2+-NH+ 4 -Na+-SO2− 4 -NO− 3 -Cl−-H2O aerosols, Atmos.
670 Chem. Phys., 7(17), 4639–4659, doi:10.5194/acp-7-4639-2007, 2007.

671 Freyer, H. D.: Seasonal variation of 15N/14N ratios in atmospheric nitrate species, Tellus B, 43(1),
672 30–44, doi:10.1034/j.1600-0889.1991.00003.x, 1991.

673 Freyer, H. D., Kley, D., Volz-Thomas, A. and Kobel, K.: On the interaction of isotopic exchange
674 processes with photochemical reactions in atmospheric oxides of nitrogen, J. Geophys. Res., 98(D8),
675 14791, doi:10.1029/93JD00874, 1993.

676 Guha, T., Lin, C. T., Bhattacharya, S. K., Mahajan, A. S., Ou-Yang, C.-F., Lan, Y.-P., Hsu, S. C. and
677 Liang, M.-C.: Isotopic ratios of nitrate in aerosol samples from Mt. Lulin, a high-altitude station in
678 Central Taiwan, Atmos. Environ., 154, 53–69, doi:10.1016/J.ATMOSENV.2017.01.036, 2017.

679 Hallquist, M., Stewart, D. J., Stephenson, S. K. and Anthony Cox, R.: Hydrolysis of N2O5 on sub-
680 micron sulfate aerosols, Phys. Chem. Chem. Phys., 5(16), 3453, doi:10.1039/b301827j, 2003.

681 He, P., Xie, Z., Chi, X., Yu, X., Fan, S., Kang, H., Liu, C. and Zhan, H.: Atmospheric Δ17O(NO3-)
682 reveals nocturnal chemistry dominates nitrate production in Beijing haze, Atmos. Chem. Phys.,
683 18(19), 14465–14476, doi:10.5194/acp-18-14465-2018, 2018.

684 He, P., Xie, Z., Yu, X., Wang, L., Kang, H. and Yue, F.: The observation of isotopic compositions of

https://doi.org/10.5194/acp-2021-487
Preprint. Discussion started: 19 July 2021


Atmospheric Chemistry and Physics Discussions

685 atmospheric nitrate in Shanghai China and its implication for reactive nitrogen chemistry, Sci. Total
686 Environ., 714, 136727, doi:10.1016/J.SCITOTENV.2020.136727, 2020.

687 Heaton, T. H. E.: 15N/14N ratios of NOx from vehicle engines and coal-fired power stations, Tellus
688 B, 42(3), 304–307, doi:10.1034/j.1600-0889.1990.00007.x-i1, 1990.

689 Kamezaki, K., Hattori, S., Iwamoto, Y., Ishino, S., Furutani, H., Miki, Y., Uematsu, M., Miura, K.
690 and Yoshida, N.: Tracing the sources and formation pathways of atmospheric particulate nitrate over
691 the Pacific Ocean using stable isotopes, Atmos. Environ., 209, 152–166,
692 doi:10.1016/J.ATMOSENV.2019.04.026, 2019.

693 Kang, H., Zhu, B., Gao, J., He, Y., Wang, H., Su, J., Pan, C., Zhu, T. and Yu, B.: Potential impacts of
694 cold frontal passage on air quality over the Yangtze River Delta, China, Atmos. Chem. Phys., 19(6),
695 3673–3685, doi:10.5194/acp-19-3673-2019, 2019.

696 Kawashima, H.: Seasonal trends of the stable nitrogen isotope ratio in particulate nitrogen compounds
697 and their gaseous precursors in Akita, Japan, Tellus B Chem. Phys. Meteorol., 71(1), 1627846,
698 doi:10.1080/16000889.2019.1627846, 2019.

699 Kim, H., Zhang, Q. and Sun, Y.: Measurement report: Characterization of severe spring haze episodes
700 and influences of long-range transport in the Seoul metropolitan area in March 2019, Atmos. Chem.
701 Phys., 20(19), 11527–11550, doi:10.5194/acp-20-11527-2020, 2020a.

702 Kim, H. C., Kim, S., Lee, S.-H., Kim, B.-U. and Lee, P.: Fine-Scale Columnar and Surface NOx
703 Concentrations over South Korea: Comparison of Surface Monitors, TROPOMI, CMAQ and CAPSS
704 Inventory, Atmosphere (Basel)., 11(1), 101, doi:10.3390/atmos11010101, 2020b.

705 Kim, S.-W., Yoon, S.-C., Kim, J. and Kim, S.-Y.: Seasonal and monthly variations of columnar
706 aerosol optical properties over east Asia determined from multi-year MODIS, LIDAR, and
707 AERONET Sun/sky radiometer measurements, Atmos. Environ., 41(8), 1634–1651,
708 doi:10.1016/j.atmosenv.2006.10.044, 2007.

709 Lee, H.-J., Jo, H.-Y., Kim, S.-W., Park, M.-S. and Kim, C.-H.: Impacts of atmospheric vertical
710 structures on transboundary aerosol transport from China to South Korea, Sci. Rep., 9(1), 13040,
711 doi:10.1038/s41598-019-49691-z, 2019.

712 Lelieveld, J., Evans, J. S., Fnais, M., Giannadaki, D. and Pozzer, A.: The contribution of outdoor air
713 pollution sources to premature mortality on a global scale, Nature, 525(7569), 367–371,

https://doi.org/10.5194/acp-2021-487
Preprint. Discussion started: 19 July 2021


Atmospheric Chemistry and Physics Discussions

714 doi:10.1038/nature15371, 2015.

715 Li, D. and Wang, X.: Nitrogen isotopic signature of soil-released nitric oxide (NO) after fertilizer
716 application, Atmos. Environ., 42(19), 4747–4754, doi:10.1016/j.atmosenv.2008.01.042, 2008.

717 Li, H., Zhang, Q., Zheng, B., Chen, C., Wu, N., Guo, H., Zhang, Y., Zheng, Y., Li, X. and He, K.:
718 Nitrate-driven urban haze pollution during summertime over the North China Plain, Atmos. Chem.
719 Phys., 18(8), 5293–5306, doi:10.5194/acp-18-5293-2018, 2018.

720 Li, J., Zhang, X., Orlando, J., Tyndall, G. and Michalski, G.: Quantifying the nitrogen isotope effects
721 during photochemical equilibrium between NO and NO2: Implications for δ15N in tropospheric
722 reactive nitrogen, Atmos. Chem. Phys., 20(16), 9805–9819, doi:10.5194/acp-20-9805-2020, 2020.

723 Li, J., Davy, P., Harvey, M., Katzman, T., Mitchell, T. and Michalski, G.: Nitrogen isotopes in nitrate
724 aerosols collected in the remote marine boundary layer: Implications for nitrogen isotopic
725 fractionations among atmospheric reactive nitrogen species, Atmos. Environ., 245, 118028,
726 doi:10.1016/j.atmosenv.2020.118028, 2021.

727 Li, Z., Walters, W. W., Hastings, M. G., Zhang, Y., Song, L., Liu, D., Zhang, W., Pan, Y., Fu, P. and
728 Fang, Y.: Nitrate Isotopic Composition in Precipitation at a Chinese Megacity: Seasonal Variations,
729 Atmospheric Processes, and Implications for Sources, Earth Sp. Sci., 6(11), 2200–2213,
730 doi:10.1029/2019EA000759, 2019.

731 Lim, S., Lee, M., Czimczik, C. I., Joo, T., Holden, S., Mouteva, G., Santos, G. M., Xu, X., Walker, J.,
732 Kim, S., Kim, H. S., Kim, S. and Lee, S.: Source signatures from combined isotopic analyses of
733 PM2.5 carbonaceous and nitrogen aerosols at the peri-urban Taehwa Research Forest, South Korea in
734 summer and fall, Sci. Total Environ., 655, 1505–1514, doi:10.1016/j.scitotenv.2018.11.157, 2019.

735 Lim, S., Yang, X., Lee, M., Li, G., Gao, Y., Shang, X., Zhang, K., Czimczik, C. I., Xu, X., Bae, M.-
736 S., Moon, K.-J. and Jeon, K.: Fossil-driven secondary inorganic PM2.5 enhancement in the North
737 China Plain: Evidence from carbon and nitrogen isotopes, Environ. Pollut., 266, 115163,
738 doi:10.1016/J.ENVPOL.2020.115163, 2020.

739 Liu, X.-Y., Yin, Y.-M. and Song, W.: Nitrogen Isotope Differences between Major Atmospheric NO
740 y Species: Implications for Transformation and Deposition Processes, Environ. Sci. Technol. Lett.,
741 7(4), 227–233, doi:10.1021/acs.estlett.0c00105, 2020.

742 Liu, Z., Gao, W., Yu, Y., Hu, B., Xin, J., Sun, Y., Wang, L., Wang, G., Bi, X., Zhang, G., Xu, H.,

https://doi.org/10.5194/acp-2021-487
Preprint. Discussion started: 19 July 2021


Atmospheric Chemistry and Physics Discussions

743 Cong, Z., He, J., Xu, J. and Wang, Y.: Characteristics of PM2.5 mass concentrations and chemical
744 species in urban and background areas of China: emerging results from the CARE-China network,
745 Atmos. Chem. Phys., 18(12), 8849–8871, doi:10.5194/acp-18-8849-2018, 2018.

746 Michalski, G. and Bhattacharya, S. K.: The role of symmetry in the mass independent isotope effect in
747 ozone, Proc. Natl. Acad. Sci., 106(14), 5493–5496, doi:10.1073/PNAS.0812755106, 2009.

748 Michalski, G., Scott, Z., Kabiling, M. and Thiemens, M. H.: First measurements and modeling of Δ^{17}
749 O in atmospheric nitrate, Geophys. Res. Lett., 30(16), doi:10.1029/2003GL017015, 2003.

750 Morin, S., Savarino, J., Frey, M. M., Domine, F., Jacobi, H.-W., Kaleschke, L. and Martins, J. M. F.:
751 Comprehensive isotopic composition of atmospheric nitrate in the Atlantic Ocean boundary layer
752 from 65°S to 79°N, J. Geophys. Res., 114(D5), D05303, doi:10.1029/2008JD010696, 2009.

753 Morin, S., Sander, R. and Savarino, J.: Simulation of the diurnal variations of the oxygen isotope
754 anomaly (Δ 17 O) of reactive atmospheric species, Atmos. Chem. Phys., 11(8), 3653–3671,
755 doi:10.5194/acp-11-3653-2011, 2011.

756 Nelson, D. M., Tsunogai, U., Ding, D., Ohyama, T., Komatsu, D. D., Nakagawa, F., Noguchi, I. and
757 Yamaguchi, T.: Triple oxygen isotopes indicate urbanization affects sources of nitrate in wet and dry
758 atmospheric deposition, Atmos. Chem. Phys., 18(9), 6381–6392, doi:10.5194/acp-18-6381-2018,
759 2018.

760 NIER: Improvement of Air Quality Forecast Based on the Measurement –Focused on Secondary
761 Formation of Nitrate NIER-SP2019-088, Incheon., 2019.

762 Park, J.: Acidity and liquid water content of PM2.5 in Seoul estimated from long-term measurements,
763 Korea University., 2021.

764 Park, Y., Park, K., Kim, H., Yu, S., Noh, S., Kim, M., Kim, J., Ahn, J., Lee, M., Seok, K. and Kim,
765 Y.: Characterizing isotopic compositions of TC-C, NO3−-N, and NH4+-N in PM2.5 in South Korea:
766 Impact of China's winter heating, Environ. Pollut., 233, 735–744,
767 doi:10.1016/J.ENVPOL.2017.10.072, 2018.

768 Parnell, A. C., Inger, R., Bearhop, S. and Jackson, A. L.: Source Partitioning Using Stable Isotopes:
769 Coping with Too Much Variation, edited by S. Rands, PLoS One, 5(3), e9672,
770 doi:10.1371/journal.pone.0009672, 2010.

https://doi.org/10.5194/acp-2021-487
Preprint. Discussion started: 19 July 2021

771 Parnell, A. C., Phillips, D. L., Bearhop, S., Semmens, B. X., Ward, E. J., Moore, J. W., Jackson, A.
772 L., Grey, J., Kelly, D. J. and Inger, R.: Bayesian stable isotope mixing models, Environmetrics, 24(6),
773 387–399, doi:10.1002/env.2221, 2013.

774 Quan, J., Dou, Y., Zhao, X., Liu, Q., Sun, Z., Pan, Y., Jia, X., Cheng, Z., Ma, P., Su, J., Xin, J. and
775 Liu, Y.: Regional atmospheric pollutant transport mechanisms over the North China Plain driven by
776 topography and planetary boundary layer processes, Atmos. Environ., 221, 117098,
777 doi:10.1016/J.ATMOSENV.2019.117098, 2020.

778 Rose, L. A., Yu, Z., Bain, D. J. and Elliott, E. M.: High resolution, extreme isotopic variability of
779 precipitation nitrate, Atmos. Environ., 207, 63–74, doi:10.1016/J.ATMOSENV.2019.03.012, 2019.

780 Saunders, S. M., Jenkin, M. E., Derwent, R. G. and Pilling, M. J.: Protocol for the development of the
781 Master Chemical Mechanism, MCM v3 (Part A): Tropospheric degradation of non-aromatic volatile
782 organic compounds, Atmos. Chem. Phys., 3(1), 161–180, doi:10.5194/acp-3-161-2003, 2003.

783 Savarino, J., Kaiser, J., Morin, S., Sigman, D. M. and Thiemens, M. H.: Nitrogen and oxygen isotopic
784 constraints on the origin of atmospheric nitrate in coastal Antarctica, Atmos. Chem. Phys., 7(8),
785 1925–1945, doi:10.5194/acp-7-1925-2007, 2007.

786 Savarino, J., Morin, S., Erbland, J., Grannec, F., Patey, M. D., Vicars, W., Alexander, B. and
787 Achterberg, E. P.: Isotopic composition of atmospheric nitrate in a tropical marine boundary layer.,
788 Proc. Natl. Acad. Sci. U. S. A., 110(44), 17668–73, doi:10.1073/pnas.1216639110, 2013.

789 Shao, P., Tian, H., Sun, Y., Liu, H., Wu, B., Liu, S., Liu, X., Wu, Y., Liang, W., Wang, Y., Gao, J.,
790 Xue, Y., Bai, X., Liu, W., Lin, S. and Hu, G.: Characterizing remarkable changes of severe haze
791 events and chemical compositions in multi-size airborne particles (PM1, PM2.5 and PM10) from
792 January 2013 to 2016–2017 winter in Beijing, China, Atmos. Environ., 189, 133–144,
793 doi:10.1016/J.ATMOSENV.2018.06.038, 2018.

794 Sharma, H. D., Jervis, R. E. and Wong, K. Y.: Isotopic exchange reactions in nitrogen oxides, J. Phys.
795 Chem., 74(4), 923–933, doi:10.1021/j100699a044, 1970.

796 Shi, C., Nduka, I. C., Yang, Y., Huang, Y., Yao, R., Zhang, H., He, B., Xie, C., Wang, Z. and Yim, S.
797 H. L.: Characteristics and meteorological mechanisms of transboundary air pollution in a persistent
798 heavy PM2.5 pollution episode in Central-East China, Atmos. Environ., 223, 117239,
799 doi:10.1016/J.ATMOSENV.2019.117239, 2020.

https://doi.org/10.5194/acp-2021-487
Preprint. Discussion started: 19 July 2021

Atmospheric Chemistry and Physics Discussions

800 Song, W., Wang, Y.-L., Yang, W., Sun, X.-C., Tong, Y.-D., Wang, X.-M., Liu, C.-Q., Bai, Z.-P. and
801 Liu, X.-Y.: Isotopic evaluation on relative contributions of major NOx sources to nitrate of PM2.5 in
802 Beijing, Environ. Pollut., 248, 183–190, doi:10.1016/J.ENVPOL.2019.01.081, 2019.

803 Song, W., Liu, X.-Y., Wang, Y.-L., Tong, Y.-D., Bai, Z.-P. and Liu, C.-Q.: Nitrogen isotope
804 differences between atmospheric nitrate and corresponding nitrogen oxides: A new constraint using
805 oxygen isotopes, Sci. Total Environ., 701, 134515, doi:10.1016/J.SCITOTENV.2019.134515, 2020.

806 Stein, A. F., Draxler, R. R., Rolph, G. D., Stunder, B. J. B., Cohen, M. D. and Ngan, F.: NOAA's
807 HYSPLIT Atmospheric Transport and Dispersion Modeling System, Bull. Am. Meteorol. Soc.,
808 96(12), 2059–2077, doi:10.1175/BAMS-D-14-00110.1, 2015.

809 Thiemens, M. H.: HISTORY AND APPLICATIONS OF MASS-INDEPENDENT ISOTOPE
810 EFFECTS, Annu. Rev. Earth Planet. Sci., 34(1), 217–262,
811 doi:10.1146/annurev.earth.34.031405.125026, 2006.

812 Tong, D., Zhang, Q., Liu, F., Geng, G., Zheng, Y., Xue, T., Hong, C., Wu, R., Qin, Y., Zhao, H., Yan,
813 L. and He, K.: Current Emissions and Future Mitigation Pathways of Coal-Fired Power Plants in
814 China from 2010 to 2030, Environ. Sci. Technol., 52(21), 12905–12914, doi:10.1021/acs.est.8b02919,
815 2018.

816 Vicars, W. C. and Savarino, J.: Quantitative constraints on the 17O-excess (Δ17O) signature of
817 surface ozone: Ambient measurements from 50°N to 50°S using the nitrite-coated filter technique,
818 Geochim. Cosmochim. Acta, 135, 270–287, doi:10.1016/J.GCA.2014.03.023, 2014.

819 Vicars, W. C., Bhattacharya, S. K., Erbland, J. and Savarino, J.: Measurement of the 17O-excess
820 (Δ17O) of tropospheric ozone using a nitrite-coated filter, Rapid Commun. Mass Spectrom., 26(10),
821 1219–1231, doi:10.1002/rcm.6218, 2012.

822 Wahner, A., Mentel, T. F., Sohn, M. and Stier, J.: Heterogeneous reaction of N_2O_5 on sodium nitrate
823 aerosol, J. Geophys. Res. Atmos., 103(D23), 31103–31112, doi:10.1029/1998JD100022, 1998.

824 Walters, W. W. and Michalski, G.: Theoretical calculation of nitrogen isotope equilibrium exchange
825 fractionation factors for various NOy molecules, Geochim. Cosmochim. Acta, 164, 284–297,
826 doi:10.1016/J.GCA.2015.05.029, 2015.

827 Walters, W. W. and Michalski, G.: Theoretical calculation of oxygen equilibrium isotope
828 fractionation factors involving various NO molecules, OH, and H2O and its implications for isotope

https://doi.org/10.5194/acp-2021-487
Preprint. Discussion started: 19 July 2021


Atmospheric Chemistry and Physics Discussions

variations in atmospheric nitrate, Geochim. Cosmochim. Acta, 191, 89–101, doi:10.1016/j.gca.2016.06.039, 2016.

Walters, W. W., Goodwin, S. R. and Michalski, G.: Nitrogen Stable Isotope Composition (δ^{15}N) of Vehicle-Emitted NO_x, Environ. Sci. Technol., 49(4), 2278–2285, doi:10.1021/es505580v, 2015.

Walters, W. W., Simonini, D. S. and Michalski, G.: Nitrogen isotope exchange between NO and NO_2 and its implications for δ^{15}N variations in tropospheric NO_x and atmospheric nitrate, Geophys. Res. Lett., 43(1), 440–448, doi:10.1002/2015GL066438, 2016.

Walters, W. W., Fang, H. and Michalski, G.: Summertime diurnal variations in the isotopic composition of atmospheric nitrogen dioxide at a small midwestern United States city, Atmos. Environ., 179, 1–11, doi:10.1016/J.ATMOSENV.2018.01.047, 2018.

Wang, Y., Wang, Y., Wang, L., Petäjä, T., Zha, Q., Gong, C., Li, S., Pan, Y., Hu, B., Xin, J. and Kulmala, M.: Increased inorganic aerosol fraction contributes to air pollution and haze in China, Atmos. Chem. Phys., 19(9), 5881–5888, doi:10.5194/acp-19-5881-2019, 2019a.

Wang, Y., Song, W., Yang, W., Sun, X., Tong, Y., Wang, X., Liu, C., Bai, Z. and Liu, X.: Influences of Atmospheric Pollution on the Contributions of Major Oxidation Pathways to $PM_{2.5}$ Nitrate Formation in Beijing, J. Geophys. Res. Atmos., 124(7), 4174–4185, doi:10.1029/2019JD030284, 2019b.

van der Werf, G. R., Randerson, J. T., Giglio, L., Collatz, G. J., Mu, M., Kasibhatla, P. S., Morton, D. C., DeFries, R. S., Jin, Y. and van Leeuwen, T. T.: Global fire emissions and the contribution of deforestation, savanna, forest, agricultural, and peat fires (1997–2009), Atmos. Chem. Phys., 10(23), 11707–11735, doi:10.5194/acp-10-11707-2010, 2010.

Xie, Y., Dai, H., Zhang, Y., Wu, Y., Hanaoka, T. and Masui, T.: Comparison of health and economic impacts of PM2.5 and ozone pollution in China, Environ. Int., 130, 104881, doi:10.1016/J.ENVINT.2019.05.075, 2019.

Xu, W., Sun, Y., Wang, Q., Zhao, J., Wang, J., Ge, X., Xie, C., Zhou, W., Du, W., Li, J., Fu, P., Wang, Z., Worsnop, D. R. and Coe, H.: Changes in Aerosol Chemistry From 2014 to 2016 in Winter in Beijing: Insights From High-Resolution Aerosol Mass Spectrometry, J. Geophys. Res. Atmos., 124(2), 1132–1147, doi:10.1029/2018JD029245, 2019.

Yu, Z. and Elliott, E. M.: Novel method for nitrogen isotopic analysis of soil-emitted nitric oxide,

https://doi.org/10.5194/acp-2021-487
Preprint. Discussion started: 19 July 2021

Atmospheric Chemistry and Physics Discussions

Environ. Sci. Technol., 51(11), 6268–6278, doi:10.1021/acs.est.7b00592, 2017.

Zhao, H., Zhang, X., Zhang, S., Chen, W., Tong, D., Xiu, A., Zhao, H., Zhang, X., Zhang, S., Chen, W., Tong, D. Q. and Xiu, A.: Effects of Agricultural Biomass Burning on Regional Haze in China: A Review, Atmosphere (Basel)., 8(12), 88, doi:10.3390/atmos8050088, 2017.

Zheng, H., Kong, S., Wu, F., Cheng, Y., Niu, Z., Zheng, S., Yang, G., Yao, L., Yan, Q., Wu, J., Zheng, M., Chen, N., Xu, K., Yan, Y., Liu, D., Zhao, D., Zhao, T., Bai, Y., Li, S. and Qi, S.: Intra-regional transport of black carbon between the south edge of the North China Plain and central China during winter haze episodes, Atmos. Chem. Phys., 19(7), 4499–4516, doi:10.5194/acp-19-4499-2019, 2019.

Zong, Z., Wang, X., Tian, C., Chen, Y., Fang, Y., Zhang, F., Li, C., Sun, J., Li, J. and Zhang, G.: First assessment of NOx sources at a regional background site in north China using isotopic analysis linked with modeling, Environ. Sci. Technol., 51(11), 5923–5931, doi:10.1021/acs.est.6b06316, 2017.

Zong, Z., Tan, Y., Wang, X., Tian, C., Li, J., Fang, Y., Chen, Y., Cui, S. and Zhang, G.: Dual-modelling-based source apportionment of NOx in five Chinese megacities: Providing the isotopic footprint from 2013 to 2014, Environ. Int., 137, 105592, doi:10.1016/J.ENVINT.2020.105592, 2020.